*Journal of Applied Polymer Science*

WILEY

Applied Polymer SCIENCE

RESEARCH ARTICLE

# Influence of Green Nanofillers on the Morphological, Mechanical Properties, and Degradation Kinetics of PBS/PBAT Blends: A Potential Sustainable Strategy for Fisheries Applications

Yousra Nait Hamou[1,2] | Samira Benali[1] | Mostapha Benomar[3] | Sandro Gennen[4] | Jean-Michel Thomassin[4] | Job Tchoumtchoua[4] | Hassan Er-Raioui[2] | Jean-Marie Raquez[1]

[1]University of Mons (UMONS) - Laboratory of Polymeric and Composite Materials (LPCM), Center of Innovation and Research in Materials and Polymers (CIRMAP), Mons, Belgium | [2]Laboratory of Environment, Oceanology and Natural Resources, Department of Earth Sciences, Faculty of Sciences and Technologies, Tangier Abdelmalek Essaadi University, Tangier, Morocco | [3]National Institute of Halieutic Research (INRH), Dradeb Tangier, Morocco | [4]Celabor Srl, Herve, Belgium

**Correspondence:** Samira Benali (samira.benali@umons.ac.be)

**Received:** 17 October 2024 | **Revised:** 30 January 2025 | **Accepted:** 19 February 2025

**Funding:** This work is supported by "Académie de Recherche et d'Enseignement supérieur, (ARES)" in the framework of Research & Development Project (2022–2027 Program) between Belgium and European Regional Development Fund (ERDF-FEDER) for general support in the frame of UP_PLASTICS portofolio. Jean-Marie Raquez is an F.R.S.-FNRS Research Associate.

**Keywords:** biopolymers and renewable polymers | blends | mechanical properties | nanoparticles | nanowires and nanocrystals | structure-property relationships

## ABSTRACT

Synthetic nylon fishing nets pose significant threats to marine ecosystems, contributing to ghost fishing and microplastic pollution. While the development of biodegradable polymers for marine applications has progressed, significant challenges remain in achieving the mechanical performance required for fishing nets, particularly under water conditions. This study addresses these challenges by investigating the incorporation of nanochitin and nanocellulose fillers into PBS/PBAT blends, aiming to optimize their mechanical properties and to control the degradation behavior for marine environments. First, various PBS/PBAT nanocomposites were prepared with chitin and cellulose nanofillers, and tensile tests identified the most effective fillers for mechanical reinforcement. Differential scanning calorimetry (DSC), size exclusion chromatography (SEC), and scanning electron microscopy (SEM). The results demonstrated significant mechanical reinforcement in air conditions, with efficient nanofiller dispersion, particularly in two nanocomposites: PBS/PBAT/ChNCs—$Lac_{1\%}$ and PBS/PBAT/NFC—$Ester_{1\%}$. These formulations exhibited notable improvements in mechanical properties compared to the other blends. Specifically, Young's modulus increased by +15% and + 22%, respectively, while elongation at break improved by +10% and + 7%, respectively. Under aqueous conditions, PBS/PBAT/ChNCs—$Lac_{1\%}$ also showed a remarkable +52% increase in elongation at break. Additionally, weathering tests were also examined the nanofillers' influence on degradation kinetics, revealing that chitin nanofillers accelerated degradation under controlled conditions. These findings suggest that while nanochitins and nanocelluloses improve mechanical properties in certain environments, further research is required to optimize their performance in water.

## 1 | Introduction

Since the 1950s, plastic fishing nets have offered a means of improving fishing efficiency with a longer lifetime. However, while they are appreciated by fishermen, they are also considered among the main sources of plastic waste in the marine environment. In 2018, the European Commission reported that Abandoned, Lost, Discarded Fishing Gear (ALDFG) constitutes around 27% of plastic marine litter and around 70% of the total marine litter items [1]. Furthermore, these fishing nets can cause many environmental problems after their loss or abandonment in the seas, such as the phenomenon of ghost fishing [2] by extending to trap marine animals or the intoxication of marine animals by plastic debris and their additives.

In recent years, new green materials derived from natural sources, which are biodegradable over time, have been widely studied and developed and are currently being employed to replace several other synthetic polymers, that is, obtained from petroleum sources, in different fields such as plastic packaging, agriculture, and biomedical applications [3, 4].

Many researchers are interested in finding alternative green materials to replace synthetic fishing nets made of polyamide-6. Some of these researchers have explored the effectiveness of polylactide (PLA) nets [5], but the biodegradability of PLA under marine environments remains a main issue [6]. In 2007, Park et al. conducted the first investigations on biodegradable monofilaments made of polybutylene succinate (PBS) [7] with promising developments.

PBS is an aliphatic polyester synthesized from succinic acid (SA) and 1,4-butanediol (BDO). It can be petrosourced or semi-biosourced. Mitsubishi Chemical Corporation (Japan), in collaboration with PTT Public Company Limited (Thailand), introduced BioPBS to the market in 2017. BioPBS is synthesized from a biosourced SA–(the method for synthesizing a biobased SA developed by researchers in the recent decades consists of microbial fermentation using different carbohydrate sources, including sugars from sucrose, starch crops, and lignocellulosic materials [8, 9]). BDO, on the other hand, is still produced using traditional petrochemical methods. However, researchers and several large producers of BDO continue to investigate alternative green methods by employing renewable resources to synthesize bio-BDO [10].

PBS is a promising material because it has outstanding thermal and mechanical properties (mechanical strength and toughness), is easily processed, and has a relatively low cost. Another benefit of this polymer is its biodegradability under specific environmental conditions, such as home composting using high temperatures (above 30°C) and humid environments. It can also be degraded in marine environments, which is considered an exceptional property that can reduce the ghost fishing phenomenon and marine pollution [11–13].

The first studies realized on biodegradable monofilaments prepared using PBS have shown good physical properties, such as tensile strength that should be sufficient to withstand the physical stresses associated with fishing applications, and elasticity and flexibility that ensure good handling of water currents and captured fish without breaking. They are also durable for the time required to perform fishing activities and resist abrasion. PBS monofilaments have also been shown to retain a significant proportion of their strength even when knotted, which is critical for maintaining the function of the nets over time [7]. Overall, while PBS monofilaments offer the advantage of biodegradability and outstanding mechanical properties in dry conditions, their performance in wet environments is reduced due to changes in their mechanical properties when exposed to water. This was shown by the decrease of tensile strength, which affects the net's ability to withstand the stresses of fishing operations, as well as the increase in the elongation at break, the extent of which is considered excessive and could result in larger mesh sizes under stress that might allow fish to escape, or could lead to the entanglement of other marine species, thereby increasing the risk of ghost fishing [14, 15].

In order to improve the mechanical properties of these biodegradable monofilaments, Park et al., as well as other researchers, have shifted their focus to the melt blend derived from PBS/polybutylene adipate terephthalate (PBAT) to manufacture the nets [16 17]. PBAT is an aromatic copolyester synthesized from adipic acid, terephthalic acid, and BDO. Its synthesis still relies on petrochemical resources; however, its ability to decompose in appropriate composting conditions and its biodegradability in marine conditions compared to other biosourced and biodegradable polymers make it an environmentally friendly alternative to synthetic plastics [18]. Due to its biodegradability and excellent mechanical properties, such as elasticity, PBAT has already been used in different applications, such as in agricultural mulch films, compostable bags, and packaging materials, and it is often used in blends with other biopolymers to improve their mechanical properties and accelerate their biodegradation [19].

As PBS/PBAT blends started to earn the attention of many researchers in fisheries applications, the studies realized in this field showed an improvement in mechanical properties compared to PBS. The improvements observed were higher flexibility, enhancement of impact strength and toughness, and better processability. These properties are crucial to maintaining the durability and performance of biodegradable fishing nets facing stresses, dynamic loads, and movements of water and marine life without breaking. However, the results in marine conditions indicate some limits for fishing efficiency due to the problems of mechanical resistance after immersion [16, 20–22].

Despite the improvement of mechanical and physical properties of PBS/PBAT blends, especially in contact with water, researchers have developed some approaches to attempt to reinforce the PBS/PBAT blend at nanoscales by performing reactive extrusion. This improves the compatibility through a transesterification reaction, as shown in the study of Muthuraj et al. [23]. The blends, however, still exhibited phase separation and a decrease in the molecular weight due to the breakdown of polymer chains during transesterification that can potentially affect the mechanical properties of the blend. Another approach that has been supported by many researchers in different fields is the incorporation of specific

nanofillers within polymeric matrices that can ensure more compatibility and improvement of physical and mechanical properties. In the case of PBS/PBAT, the literature presents few research studies using nanofillers with PBS/PBAT in several fields. For instance, using lignin and zinc oxide (ZnO) nanoparticles can adjust mechanical properties, including tensile strength, and add some other functionalities to the blend, such as self-cleaning and antimicrobial properties useful in biomedical applications [24]. Another study, which used silicon dioxide ($SiO_2$) as a compatibilizer agent of the PBS/PBAT blend, showed an improvement in the mechanical, viscosity, and barrier properties of the composite films designed for food packaging applications [25].

Most of the studies agree that the complex behavior of incompatible PBS/PBAT blends behaves differently with each nanofiller, and its properties can depend on the ratio of each polymer as well as the nanofillers used in the blend. Despite these advancements, a critical research gap persists in developing biodegradable materials that balance mechanical performance and controlled degradation under marine conditions. This study aims to fill this gap by exploring the incorporation of bio-based nanofillers into PBS/PBAT blends. These nanofillers are hypothesized to enhance the mechanical properties while maintaining the environmental compatibility of the material, offering a sustainable solution for marine applications, particularly in the development of fishing nets.

In this regard, the strategy of our study is to investigate and understand the mechanical and morphological behavior of the polymer blend PBS/PBAT before and after adding a specific green nanofiller prepared from chitin and cellulose fibers. Due to their low cost, excellent biocompatibility, biodegradability, and antibacterial properties, nanochitins, and cellulose nanofillers are interesting nanoadditives used to enhance the physical properties of polymers. Nanosized chitin and cellulose have been successfully used in the preparation of composites with polymers [26, 27]. In the framework of stricter regulations and environmental considerations, the degradation of PBS/PBAT nanocomposites was also studied at 75°C based on an accelerated degradation protocol developed by Kanemura et al. [28]. In the frame of a balanced approach, ecotoxicology and monofilament studies will be featured in future publications.

## 2 | Experimental

### 2.1 | Materials

Polybutylene succinate (*BIOPBS FZ71 PM* grade) was supplied in pellet form by PTT MCC BIOCHEM COMPANY LIMITED-THAILAND, and according to the datasheet of the manufacturer, the polymer had a melt flow index (MFR) of 22 g·10 $min^{-1}$ measured at 190°C; 2.16 kg, density of 1.26 g $cm^{-3}$, and a melting point ($T_m$) of 115°C. Polybutylene adipate co-terephthalate (PBAT *ECOFLEX C1200* grade) was supplied in pellet form by BASF-GERMANY. The polymer had an MFR of 2.7–4.9 g 10 $min^{-1}$ measured at 190°C; 2.16 kg, density of 1.25–1.27 g $cm^{-}$, and $T_m$ of 110°C–120°C. Chitin fibers extracted from shell shrimps (commercial grade) were supplied from SIGMA-ALDRICH and then used to prepare functionalized and non-functionalized nanochitins characterized by a typical needle-shaped morphology, 500 in length and 17 nm in thickness. Cellulose fibers were extracted from the Miscanthus plant and then used to prepare the functionalized cellulose nanofillers with a particle diameter in the range of 10 to 20 nm. The Figure 1 presents the molecular structures of the polymers used in the study. The reagents, including technical grade hydrochloric acid (HCl) 37%, were supplied from PanReac AppliChem (ITW Reagents). Lactic acid ($C_3H_6O_3$) 85% FCC (code W261106-1KG-K) was purchased from Sigma-Aldrich, and synthesis grade butyric acid ($C_4H_8O$) (code 8.00457.2500) was supplied from Merck Millipore. PTFE membrane filters with a 0.22 μm pore size and 47 mm diameter were purchased from FilterLab. Molecular porous membrane tubing of the grade Spectra/por 3 dialysis membrane (standard RC tubing with MWCO: 3.5Kd, diameter: 34 mm, Nominal flat width: 54 mm) was supplied from Spectrum Laboratories. 2,2,6,6-Tetramethylpiperidine 1-oxyl, 2,2,6,6-tetramethyl-1-piperidinyloxy (TEMPO), glycidyltrimethyl ammonium chloride (EPTMAC) and NaClO (6%–14% active chlorine) are provided from Sigma-Aldrich.

### 2.2 | Method

#### 2.2.1 | Preparation of Chitin Nanocrystals

In order to ensure a better dispersion and compatibilization of nanochitins in the hydrophobic polymeric matrix, non-functionalized, and functionalized chitin nanofillers were

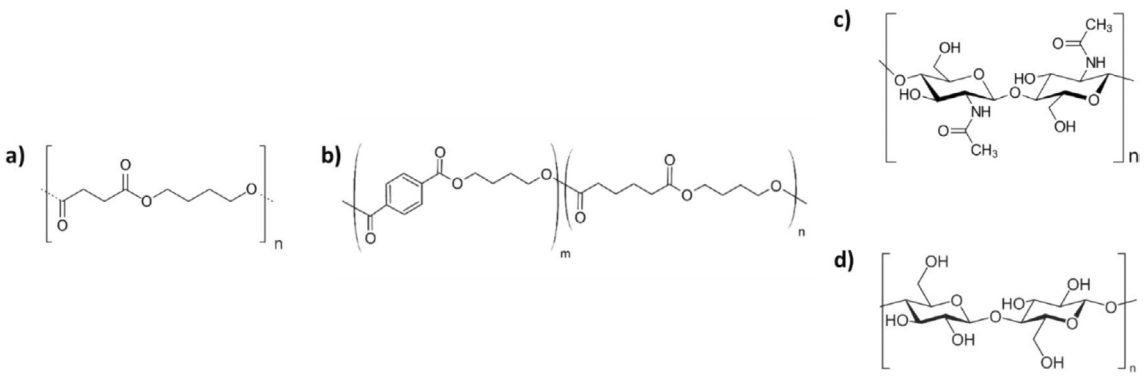


**FIGURE 1** | Chemical structure of (a) polybutylene succinate (PBS), (b) polybutylene adipate co-terephthalate (PBAT), (c) nanochitin, and (d) cellulose nanofillers. [Color figure can be viewed at wileyonlinelibrary.com]

used. The acid hydrolysis method was used to produce non-functionalized chitin nanocrystals ChNCs—HCl in the presence of HCl 12 M based on Magnani et al. [29, 30]. Ten gram of chitin were soaked in 225 mL of DI water in a three-neck round-bottom flask, and the temperature was risen to 100°C, keeping the suspension under mechanical stirring with the help of an overhead stirrer (IKA-Werke GmbH & Co. KG, Germany) equipped with a Teflon centrifugal stirrer shaft (ThermoFisher Scientific Inc., Sweden) (500 rpm). Then, 75 mL of HCl 12 M was added. After the addition of all the reagents, the chitin concentration was 30 mL/$g^{-1}$ and the final HCl concentration was 3 M. Acid hydrolysis was stopped after 90 min to increase the pH to 6; the mixture was filtered six times with a nylon membrane with pores of 0.22 μm using high-pressure filtration equipment. Each time, the cake collected from the filter was resuspended in water with the help of an T18 digital Ultra Turrax equipped with an S 18 N-19 G dispersing tool (IKA-Werke GmbH & Co. KG, Germany). To collect the nanocrystals, the suspension was centrifuged at room temperature (5 min, 3800 rpm), recovering the opalescent supernatant and resuspending the precipitate containing the unhydrolyzed chitin. The procedure was repeated 10 times, and the collected supernatants were unified and filtered with a fritted glass filter with porosity 3 to eliminate any possible residue of microchitin. The final sample was stored in a fridge at 6°C. For the functionalized ChNC preparation, one-pot acid hydrolysis/fischer esterification from Magnani et al. [30] was used. Five gram of chitin was soaked overnight in a mixture of DI water and the desired organic acid (lactic or butyric acid) at room temperature. Then, the temperature was risen until reflux (116°C for lactic acid and 107°C for butyric acid) under mechanical agitation (500 rpm) and a catalytic quantity of HCl 12 M was added to reach the desired final concentration. The final concentration of chitin was 0.04 $^{-1}$mg/mL. The reaction was stopped after 3 or 5 h, and the chitin was separated from the rest through centrifugation (8000 rpm, 15 min, and 5°C–10°C reached in a freezer). Each mixture was redispersed in DI water and filtered four times (with a nylon membrane with pores of 0.45 μm using high-pressure filtration equipment) to reach pH = 6, redispersing the cake on the filter in clean DI water using Ultra Turrax. Then, the nanocrystals were collected and separated from the unhydrolyzed chitin through centrifugation (3800 rpm, 5 min, RT), each time collecting the supernatant and resuspending the precipitate with Ultra Turrax. For each sample, this procedure was repeated 10 times. In the end, all the collected supernatants were filtered with a fritted glass filter (porosity 3) to obtain a pure sample of ChNCs.

### 2.2.2 | Preparation of Cellulose Nanofibers

**2.2.2.1 | Extraction of Misacanthus.** The extraction of fibers from Miscanthus was performed by sub-critical water extraction. The equipment used for sub-critical water extraction was a 6 L pilot scale stainless steel extractor (SEPAREX, France). A 300 g of Miscanthus (dried and milled at 4 mm) were inserted in the reactor; Milli-Q water heated up to 120°C in a separate 20 L reactor percolates through the sample in the reactor during 2 cycles of 30 min with recirculation to remove polyphenols. Then, water was alkalized with 1% NaOH, heated up to 140°C, and percolated through the residual sample in the reactor during 2 cycles of 30 min with recirculation to remove lignin. Pressure (15–17 bars) in the system was maintained at the selected temperature during the whole process by setting the pressure regulator. After the extraction, the reactor was decompressed and cooled down to reach a temperature below 30°C, and the residual cellulose was collected and further bleached to yield a whiter powder of miscanthus fibers. The bleaching process was performed using a solution of 6% NaOH and 10% $H_2O_2$ (1/1) in a solid/liquid ratio of 1/40.

**2.2.2.2 | Production of Cellulose Nanofiber Functionalized With Carboxylate Function (NFC-TEMPO).** Ten gram of Miscanthus fibers are mixed with 500 mL of water overnight before adjusting the pH to 8.5 with a solution of NaOH (0.5 M). In parallel, 1 g of NaBr and 0.166 g of 2,2,6,6-tetramethylpiperidine 1-oxyl, 2,2,6,6-Tetramethyl-1-piperidinyloxy (TEMPO) are mixed within 33.3 mL of water. The TEMPO/NaBr solution is then added to the cellulose solution before adjusting the pH to 10–11 with a solution of NaOH (0.5 M). A 33.3 mL of NaClO (6%–14% active chlorine) is then added to the solution. NaOH (0.5 M) is continuously added to the solution to keep the pH at 10–11. When the pH becomes constant, the reaction is stopped by adding 0.66 L of ethanol. After 10 min, the solution is filtered under vacuum with a 6 μm filter. The recovered solid is then added to a suspension of 4 L DI. The filtration/redispersion in 4 L deionized water is repeated 3 times to further wash the modified cellulose. The modified cellulose fiber is then suspended at 1 wt.% in deionized water and passed through a high-pressure homogenizer (GET) 9 times at 1000 bar for defibrillation.

**2.2.2.3 | Production of Cationic Cellulose Nanofiber (NFC-CAT).** Twenty gram of miscanthus fibers are blended with 80 mL of DI. The mixture is then passed 2 times through an extruder (ThermoFisher, Process 11) for predefibrillation at 20°C and 250 rpm. The dry content is then determined, and 20.4 g of cellulose (based on dry content) is blended with 250 g of deionized water before homogenization using an Ultra-Turrax equipment. The solution is then added to a 500 mL round bottom flask before the addition of 42.5 g of a NaOH solution (32%). The solution is then mixed at 65°C for 30 min. A 102 mL of glycidyltrimethyl ammonium chloride (EPTMAC) is then added, and the solution is mixed at 65°C for 5 h. The mixture is then neutralized to pH = 7 with an HCl solution before washing by repeating filtration/redispersion in 4 L of deionized water 5 times. The modified cellulose fiber is then suspended at 1 wt.% in deionized water and passed through a high-pressure homogenizer (GET) 9 times at 1000 bar for defibrillation.

**2.2.2.4 | Production of Enzymatic Cellulose Nanofiber (NFC-ENZY).** Sixteen gram of miscanthus fiber are blended in 1.1 L of DI and mixed during the night at 600 rpm using a mechanical agitator (IKA-Werk). The pH of the solution is then adjusted to 5 using glacial acetic acid and sodium acetate trihydrate. The solution is heated to 50°C, and 2.4 mL of enzyme FiberCare is added to the solution. The reaction is then mixed at 50°C during 5 h. The mixture is washed by repeating filtration/redispersion in 4 L of DI 5 times. The modified cellulose fiber is then suspended at 0.6 wt.% in DI

and passed through a high-pressure homogenizer (GET) 9 times at 1000 bar for defibrillation.

**2.2.2.5 | Production of Lauric Acid Modified Cellulose Nanofiber (NFC—Ester).** Six milliltre of anhydride acetic and 6 g of lauric acid were first mixed at 60°C for 20 min before the addition of 90 μL of $HClO_4$ and further mixing at 60°C for 1 h. The solution is then added to a mixture of 3.5 g of lyophilized NFC-ENZY within 31.5 g of acetone. The solution is then added to an extruder (ThermoFisher, Process 11) at 40°C and 50 rpm. The recovered solid is added to 150 mL of an ethanol/$H_2O$ mixture (50/50). The solid is then purified by several cycles of centrifugation at 10000 rpm for 10 min, 2 cycles with an ethanol/$H_2O$ mixture (50/50), 1 cycle with 100% ethanol, and 2 cycles with 100% acetone. The functionalization degree is then determined by IR (not showed here).

### 2.2.3 | Preparation of Nanocomposites

The highly volatile and electrostatic nanochitin, as well as cellulose nanofibers, were first mixed with barely melted PBS (approximately 90°C) in a conical flask immersed in an oil bath. After cooling, the mixtures were processed with PBAT in the DSM XPlore 15 cc extruder at a temperature of 140°C at 30 rpm for 3 min, followed by 100 rpm for 2 min before collection. The materials were then injected into the DSM Xplore mini-injector to produce dogbone-shaped specimens approximately 3 thick, 115 long, and 6 mm in width at the narrow section according to the ASTM D638 standard, which is used in mechanical and aging tests. The melt blending was preliminarily processed with 1 and 3 wt.% of ChNcs, but only samples containing 1 wt.% gave homogeneous samples. Regarding the NFC samples, 3 wt.% of NFC can be efficiently added. For a better comparison, the NFC—$Ester_{1\%}$ was also processed. The quantities used of each polymer and prepared nanofiller are expressed as weight percentages in Table 1.

### 2.2.4 | Weathering Test Protocol

The weathering test protocol was selected in accordance with the study of Kanemura et al. [28] using a single conditioning temperature of 75°C and an immersion period of 8 days to assess the degradation of the nanocomposites under more accelerated aging conditions. Nine specimens each of PBS, PBS/PBAT, and PBS/PBAT/ChNCs—$Lac_{1\%}$ with a thickness of 3 mm were immersed in test tubes filled with distilled water and placed in a stirring thermostatic bath IKA H5-B20 to maintain the temperature at 75°C throughout the experiment. Sampling was conducted on the 2ndnd, 4thth, and 8th days of the experiment, with 3 specimens being collected each time for each material. The samples were used in subsequent analyses to investigate their mechanical, morphological, and chemical properties.

### 2.2.5 | Characterization

Tensile tests were conducted under two different conditions, air and water, to evaluate the physical properties of the materials prepared before and after immersion in water. Young's modulus and elongation at break were assessed. Measurements were taken on 3 mm thick dogbone-shaped specimens injected in accordance with ASTM D638, using a ZWICK ROELL tensile tester equipped with a 2.5 kN load cell and a speed of 50 mm/min. To ensure reproducible results, five specimens were drawn for each sample in all the tensile tests conducted (under air and water), and the Young's modulus and elongation at break values were averaged across the five specimens. For *tensile tests in water*, an original protocol was confirmed after multiple experiments on the PBS/PBAT blend, and this protocol was chosen to produce the best tensile curves with a lower margin of error (standard deviation) in Young's modulus and elongation at break values. First, the specimens were soaked in distilled water for 48 h, the time at

**TABLE 1** | The ratio of biocomposites prepared with PBS/PBAT blend with the addition of nanochitins and nanocellulose obtained by different functionalizations, expressed by weight percentage.

| Biocomposites | Weight % of PBS | Weight % of PBAT | Weight % of nanochitins | Weight % of nanocellulose |
|---|---|---|---|---|
| PBS/PBAT | 82 | 18 | — | — |
| PBS/PBAT/ChNCs—$HCl_{1\%}$ | 82 | 17 | 1 | — |
| PBS/PBAT/ChNCs—$HCl_{3\%}$ | 82 | 15 | 3 | — |
| PBS/PBAT/ChNCs—$But_{1\%}$ | 82 | 17 | 1 | — |
| PBS/PBAT/ChNCs—$But_{3\%}$ | 82 | 15 | 3 | — |
| PBS/PBAT/ChNCs—$Lac_{1\%}$ | 82 | 17 | 1 | — |
| PBS/PBAT/ChNCs—$Lac_{3\%}$ | 82 | 15 | 3 | — |
| PBS/PBAT/NFC—$ENZY_{3\%}$ | 82 | 15 | — | 3 |
| PBS/PBAT/NFC—$CAT_{3\%}$ | 82 | 15 | — | 3 |
| PBS/PBAT/NFC—$TEMPO_{3\%}$ | 82 | 15 | — | 3 |
| PBS/PBAT/NFC—$Ester_{3\%}$ | 82 | 15 | — | 3 |
| PBS/PBAT/NFC—$Ester_{1\%}$ | 82 | 17 | — | 1 |

which the mixture is totally saturated with $H_2O$ molecules. After 48 h, the test specimens were removed from the water and drawn directly into the water bath connected to the tensile bench. The bath was filled with distilled water and connected to a temperature controller. All samples were assessed with water temperatures ranging from 15°C to 17°C. In the case of the samples collected during the weathering tests, the specimens (three for each material) were drawn immediately into the water after sampling to maintain the same methodology as the remaining samples. The surface morphology of the material was assessed qualitatively by scanning electron microscopy (SEM) before and after the weathering test. Pictures were taken of the surface (top view) and the cross section (edge view). For the cross section, the samples were immersed in liquid nitrogen for a few minutes and then manually fractured. Then, a 5 nm tungsten deposit was sputtered onto the samples using a Leica ACE 600 equipment. Pictures were acquired with a Hitachi SU8020 scanning electron microscope, using SE(L) and SE(U) as secondary electron detectors, at voltages of 3 and 5 kV. Using thermal analysis (TA) equipment Q2000, differential scanning calorimetry (DSC) analysis was conducted under nitrogen atmosphere at a flow rate of 50 mL/min$^{-1}$. Each sample, weighing approximately 5 to 10 mg, was placed in an aluminum pan and inserted into the device. The DSC Q2000 was carefully calibrated using indium and sapphire standards, ensuring high precision in temperature and enthalpy measurements. This controlled calibration allowed for accurate detection of thermal transitions with a resolution of ±0.1°C in temperature and ± 0.05 J g$^{-1}$ in enthalpy. A three-step procedure with a 10°C min$^{-1}$ ramp was applied including [1] heating from −80°C to 200°C and holding for 1 min to erase the thermal history, [2] cooling from 200°C to −80°C and holding for 1 min and [3] a second heating cycle from −80°C to 200°C. DSC data were analyzed using TA Instrument Universal Analysis software. Crystallinity was estimated as follows:

$$\Delta X_c = \left( \frac{\Delta H_m - \Delta H_{cc}}{\Delta H_0} \right) \times 100,$$

where $\Delta H_m$ is the enthalpy of melting, $\Delta H_{cc}$ is the enthalpy of cold crystallization and $\Delta H_0$ is the specific latent heat of the melting of the 100% crystalline polymer. For the neat resins, values of 110 and 114 J g$^{-1}$ for PBS and PBAT, respectively, were taken from the literature [31].

Size exclusion chromatography (SEC) was used to investigate the chemical stability of the prepared materials as well as variations in molecular masses during weathering experiments. Polymer solutions were prepared at 2 mg polymer/mL of $CHCl_3$. For the analysis of the molecular weight parameters, such as the number average molecular weight ($M_n$) and the dispersity ($Đ_M$), an Agilent liquid chromatograph equipped with a refractive index (RI) detector was used. A 100 µL of the samples were injected with an Agilent auto-sampler at a flow rate of 1 mL/min$^{-1}$. The calibration was performed with Polystyrene (PS) standard for separation of $M_w$ (PS) ranging from 200 to $4 \times 10^5$ g mol$^{-1}$.

## 3 | Results and Discussion

### 3.1 | Tensile Tests in Air Conditions

Tensile tests in air conditions were first carried out on the PBS/PBAT nanocomposites extruded and injected with chitin and cellulose nanofillers with different functionalizations (Figure 2). Indeed, the addition of natural nanochitin and nanocellulose fillers to the polymeric matrix may show a poor interfacial compatibility due to their higher polar character. For this purpose, the surface modification of natural nanofillers by the introduction of hydrophobic functional groups, which is widely studied in the literature and seems to be an efficient

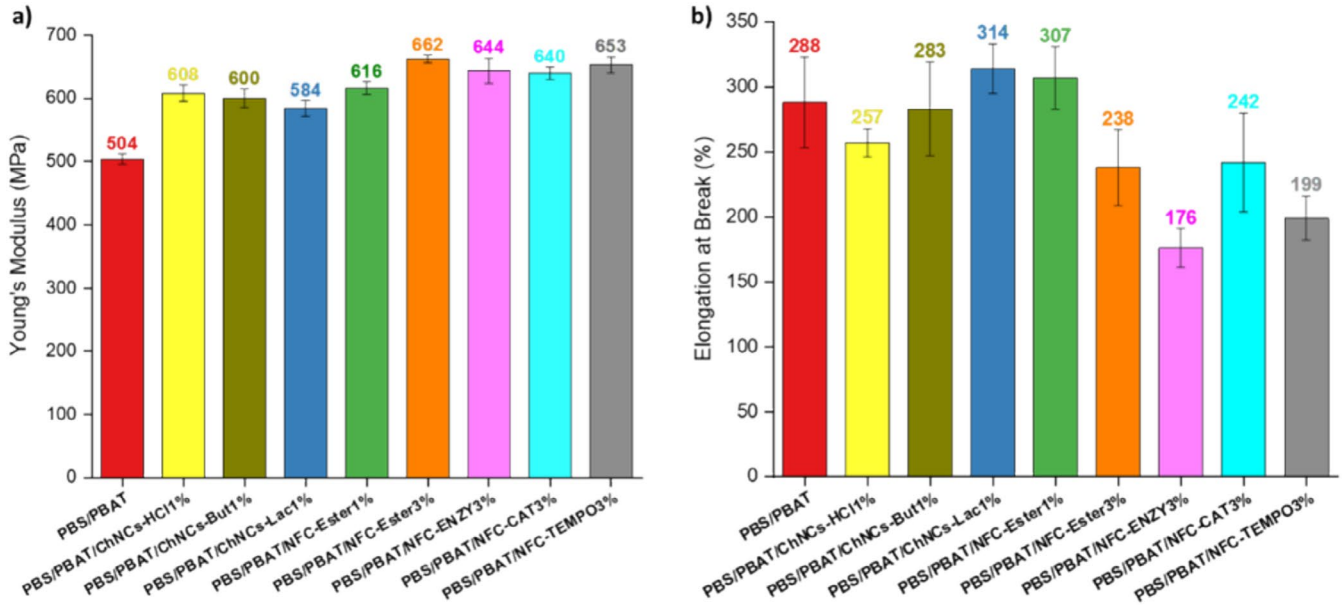


**FIGURE 2** | Graphs of tensile tests results under air conditions, comparing values obtained on (a) Young's modulus and (b) elongation at break of PBS/PBAT nanocomposites prepared with chitin nanocrystals and cellulose nanofillers. [Color figure can be viewed at wileyonlinelibrary.com]

way to solve the problem of compatibility [32], is used in this study to ensure a better compatibility with the PBS/PBAT blend. These preliminary tensile tests allowed us to assess the nanofillers, particularly in terms of mechanical enhancement in mixture with PBS/PBAT. Therefore, we were interested in Young's modulus, a mechanical value that provides information on the stiffness of the material, as well as the elongation at break, which is a mechanical measurement of the ductility and flexibility of the material. These two characteristics are critical for material selection and affect the performance of fishing nets, their handling and their durability under various environmental conditions. For example, a lower Young's modulus and higher elongation at break might be preferable to allow some stretching, accommodating larger fish catches without any breaking of the fishing nets [33, 34].

The materials were drawn in tensile test equipment using the pneumatic wedge grips for all the samples tested. Using the ASTM D638 norm with dog bone-shaped specimens, the PBS and PBAT exhibited a Young's modulus of 658 and 73 MPa, respectively, with an elongation at break of 198% and 906%, respectively, with acceptable standard deviation (For sake of the clarity, the PBS and PBAT results are not indicated in Figure 2). These values are in accordance with the technical information provided by the supplier and confirm a good process using extrusion and injection molding for homogeneous specimens.

After the same extrusion and injection process, the reference PBS/PBAT blend exhibited a Young's modulus at 504 MPa and an elongation at break at 288%. For the samples of PBS/PBAT blend with ChNCs, the Young's modulus values (Figure 2a) of PBS/PBAT/ChNCs—$HCl_{1\%}$ and PBS/PBAT/ChNCs-$But_{1\%}$ increased by approximately +20% (608 and 600 MPa for ChNCs—HCl and for ChNCs—But, respectively versus 504 MPa for PBS/PBAT blend) and by +15% for PBS/PBAT/ChNCs—$Lac_{1\%}$ (684 MPa). Regarding the samples with 3 wt.% of NFCs content, the Young's modulus values (Figure 2a) increased significantly by around +27% for the PBS/PBAT/NFC—$CAT_{3\%}$ and PBS/PBAT/NFC—$Enzy_{3\%}$ (640 and 644 MPa, respectively), +30% for PBS/PBAT/NFC—$TEMPO_{3\%}$ (653 MPa) and up to +31% for PBS/PBAT/NFC—$Ester_{3\%}$ (662 MPa). For this last result, a sample containing NFC—$Ester_{1\%}$ was also processed and exhibited an increase of +22% for the Young's modulus (616 MPa).

On the other hand, the elongation at break values (Figure 2b) of the four samples containing 3%NFCs decreased sharply by −40% for PBS/PBAT/NFC—$Enzy_{3\%}$ (176%), −31% for PBS/PBAT/NFC—$TEMPO_{3\%}$ (199%) and only around −16% for both PBS/PBAT/NFC—$CAT_{3\%}$ and PBS/PBAT/NFC—$ester_{3\%}$ (138% and 242%, respectively) showing a poor dispersion of 3 wt.% of NFCs. On the contrary, the PBS/PBAT/NFC—$ester_{1\%}$ exhibited a slight increase of +7% for elongation at break (307%). Regarding the samples containing 1 wt.% ChNCs, a slight decrease of −11% and −2% was observed for ChNCs—HCl (257%) and ChNcs—But (283%), respectively, but an increase of +10% for the elongation at break was noted for ChNCs—Lac (314%).

These outcomes allow us to focus on two blends of each category. Firstly, PBS/PBAT/ChNCs—$Lac_{1\%}$, which had a higher elongation at break (+10%) compared to the other samples and an interesting increase of Young's modulus (+15%) compared to the PBS/PBAT blend, attesting for a good interaction between nanofillers and the blend. The second blend selected is PBS/PBAT/NFC—$Ester_{1\%}$ since it presented a higher elongation at break (+7%) compared to the other melt blends with NFCs, assuming a better dispersion at lower content, as well as an increase of +22% of Young's modulus showing a nanoeffect reinforcement. These two samples will be used in further analyses to assess the mechanical behavior of these nanocomposites under water conditions. The variation in elongation at break can be attributed to the specific interactions between the PBS/PBAT matrix and the nanochitins or nanocelluloses. Taken together, these results show that Fatty acids such as lactic acid enhance the compatibility between the fillers and the matrix, leading to improved flexibility. Conversely, butyric acid, due to its bulkier structure, may restrict molecular mobility, reducing elongation. Regarding NFC samples (ester3%, enzymatic3%, CAT3%, and TEMPO3%), the variation arises from differences in surface functionalization, which impacts dispersion and interaction with the polymer matrix.

### 3.2 | Differential Scanning Analysis (DSC)

DSC analyses were conducted on the selected PBS/PBAT nanocomposites as well as on neat PBS and PBAT to better understand the crystallization rate. The crystallization behavior of polymers within nanocomposite materials is a critical parameter, as it provides valuable insights into the effects of nanofiller incorporation in PBS/PBAT blends. Crystallinity significantly influences the mechanical and thermal properties of the material: higher crystallinity typically results in enhanced tensile strength and stiffness, while lower crystallinity improves toughness and flexibility. The addition of nanofillers can alter the crystallization process by either facilitating or restricting the mobility of polymer chains, depending on their structure, dispersion, and interactions with the matrix. These changes directly affect the material's overall performance, particularly in terms of mechanical reinforcement and thermal stability [35]. The second heating cycle thermograms are presented in Figure 3. The thermal parameters are also calculated and presented in Table 2. Looking at the thermograms of the second heating ramp, we can clearly observe only one glass transition for PBS, PBAT, and the blends, which occurs at around −31°C. This can be explained by the close proximity of PBS and PBAT glass transition temperature values, so their $T_g$ signals overlap for all the PBS/PBAT nanocomposites [31]. The melt temperature, corresponding to the exotherm peak, of PBS and PBAT occurs at 115°C and 124°C with a crystallization rate of 37% and 10%, respectively. We can note the already documented small endotherm peak just before the exotherm peak for PBS corresponding to a slight cold crystallization. The cold crystallization process is very common for polyesters, and it is strictly correlated with the rate of cooling from the melt leading to metastable crystalline nuclei formation due to the increased macromolecular mobility at temperatures above the glass transition during the second heating ramp [31]. In the case of PBS, several researchers have studied the crystallization behavior of the polymer and have linked this thermal melting behavior to the polymorphism phenomenon. Indeed, PBS crystallizes according to two different crystal structures, the α and β forms. The α form appears when the PBS is crystallized from the melt, while the β form appears under

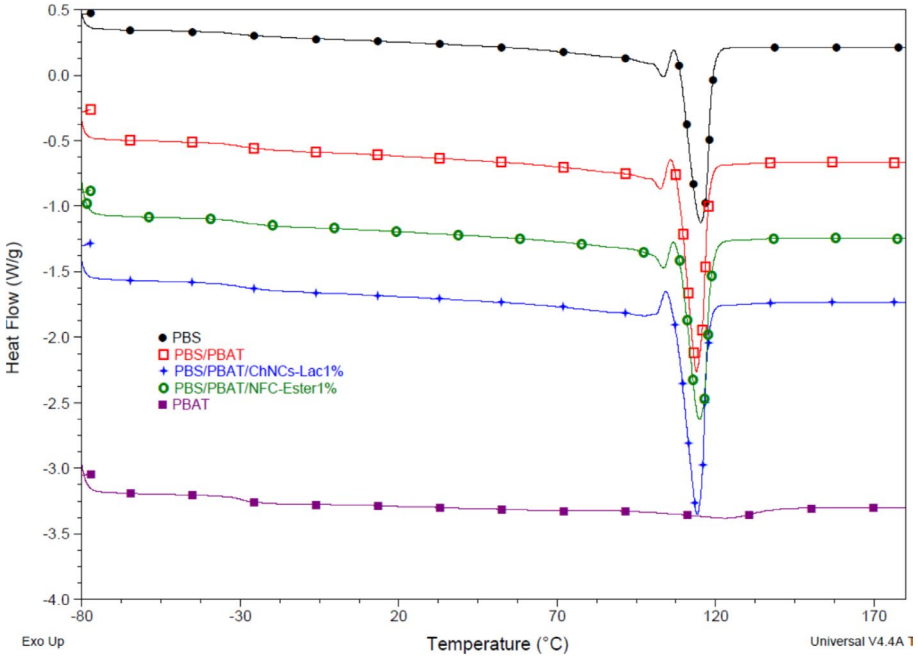


**FIGURE 3** | DSC thermograms of PBS, PBS/PBAT, PBS/PBAT/ChNCs—$Lac_{1\%}$, PBS/PBAT/NFC—$Ester_{1\%}$, and PBAT during the second heating cycle (10°C $min^{-1}$). [Color figure can be viewed at wileyonlinelibrary.com]

**TABLE 2** | DSC results for PBS, PBS/PBAT, PBS/PBAT/ChNCs—Lac1%, PBS/PBAT/1%NFC—Ester1%, and PBAT during the second heating cycle (10°C $min^{-1}$).

| Samples | $T_g$ (°C) | $T_{cc}$ (°C) | $\Delta H_{cc}$ ($J g^{-1}_{PBS}$) | $T_m$ (°C) | $\Delta H_m$ ($J g^{-1}_{PBS}$) | $\Delta H_m$ ($J g^{-1}_{PBAT}$) | $\chi_{c\,PBS}$ (%) | $\chi_{c\,PBAT}$ (%) |
|---|---|---|---|---|---|---|---|---|
| PBS | −31 | 107 | 3 | 115 | 44 | — | 37 | — |
| PBS/PBAT | −32 | 106 | 3 | 114 | 54 | — | 46 | — |
| PBS/PBAT/ ChNCs—$Lac_{1\%}$ | −30 | 107 | 4 | 115 | 44 | — | 36 | — |
| PBS/PBAT/ NFC—$Ester_{1\%}$ | −31 | 102 | 3 | 114 | 60 | — | 51 | — |
| PBAT | −30 | — | — | 124 | — | 12 | — | 10 |

mechanical stress [36, 37]. Simultaneously, some authors, such as Wang et al., have demonstrated by x-ray diffraction analysis that PBS samples crystallized at different temperatures have the same crystal structure corresponding to the α form [38]. Whereas for the PBS/PBAT blend, it has been noted that the addition of PBAT with a ratio of 18% increases the crystallization rate of PBS from 37% to 46% at similar cold crystallization and only one melting temperature. This result can be related to the morphology. The presence of a nodule of PBAT can promote the crystallization of PBS [31].

This thermal melting behavior was also observed for the PBS/PBAT nanocomposites. In the case of the PBS/PBAT/ChNCs—$Lac_{1\%}$ blend, the $T_{cc}$ remained at the same value as neat PBS, at around 107°C. The crystallization rate of the PBS/PBAT/ChNCs—$Lac_{1\%}$ blend was also similar to that of PBS (37%). The specific thermal behavior of the PBS/PBAT/ChNCs—$Lac_{1\%}$ blend has been reported in the literature. According to Fu et al. [35], who studied the thermal properties of PBS/ChNCs— nanocomposites and had the same thermal behavior results, they explained it by two major reasons. The first reason is that ChNCs have a specific rod-shaped structure, which could impact the mobility and arrangement of the molecular chains when the ChNCs are dispersed in the PBS matrix. The second reason is the interaction of the hydrogen bonds formed by the ChNCs that could also prevent the sliding of the PBS molecular chains, which implies a reduction in the crystallinity rate [35]. However, this reduction of crystals is also correlated to the morphology of the melt blend. If nodules of PBAT are also smaller and well dispersed with nanofiller (See Figure 6), crystal formation is promoted but is counterbalanced by the interaction between ChNCs and PBS, leading to a decrease in the crystallinity rate. Regarding PBS/PBAT/NFC—$Ester_{1\%}$, the $T_{cc}$ of PBS is a slightly decreased with nanocellulose fillers (102°C vs. 107°C) with a similar $T_m$ and a remarkable increase in the crystallinity rate from 37% for neat PBS to 46% for the binary melt blend and to 51% with nanocellulose fillers. This result can be directly correlated to the morphology analysis presented below (Figure 6c) showing smaller nodules promoting the PBS crystal formation.

### 3.3 | SEC Measurement of Nanocomposites

To identify physicochemical changes in the studied nanocomposites, a SEC analysis was conducted, and the values of $M_n$, $M_w$, and $Đ$ are recorded in Table 3. The neat PBS and PBAT were also analyzed before and after extrusion to verify if they exhibit degradation during their extrusion. Indeed, molecular weight is directly related to mechanical properties. Higher molecular weight leads to stronger chain entanglement, enhancing tensile strength and resistance to elongation, which are crucial for fishing nets exposed to harsh conditions. Conversely, lower molecular weight results in reduced strength, increased brittleness, and faster degradation, negatively affecting durability [23].

The molecular weight of PBS decreased significantly after the extrusion process, which reveals a degradation of the polymer when exposed to high pressure and temperature inside the extruder chamber, while the molecular weight values of PBAT almost did not change. This indicates that PBAT is more resistant and stable at higher temperatures and pressures compared to PBS. It is noted that with the addition of PBAT (18%), the molecular weight of the blend is slightly improved compared to neat PBS. On the other hand, the addition of ChNCs—Lac to the blend led to a significant improvement in its molecular weight, while the addition of NFC—Ester did not show a considerable change in the values of molecular weight.

**TABLE 3** | GPC results presented by $M_n$, $M_w$, and $Đ$ values of the nanocomposites studied.

| Samples | $M_n$ (Kg mol$^{-1}$) | $M_w$ (Kg mol$^{-1}$) | $Đ$ |
|---|---|---|---|
| PBS (non-extruded) | 45,3 | 131,7 | 2,9 |
| PBS extruded | 27,4 | 82,4 | 3,0 |
| PBAT (non-extruded) | 54,5 | 154,8 | 2,8 |
| PBAT extruded | 51,4 | 154,4 | 3,0 |
| PBS/PBAT | 34,6 | 104,5 | 3,1 |
| PBS/PBAT/ ChNCs—Lac$_{1\%}$ | 41,2 | 110,0 | 2,6 |
| PBS/PBAT/ NFC—Ester$_{1\%}$ | 36,8 | 100,6 | 2,7 |

### 3.4 | Tensile Tests in Water Conditions

The protocol of tensile tests under water conditions was elaborated to study the mechanical behavior of PBS/PBAT nanocomposites when wet and immersed in water, in order to simulate the conditions experienced by synthetic fishing nets throughout their use in seawater. In this section, all the samples in water conditions were drawn using a screw-action manual grip and were compared to those drawn in air conditions using the same grips.

In order to achieve a better understanding of the mechanical behavior of our samples and their interactions with nanochitins and nanocelluloses, we will first discuss the shape of the curves obtained from the tensile tests. The tensile tests, under air conditions, curves for PBS, PBAT, PBS/PBAT blends and their nanocomposites are shown in Figure 4a. PBAT presents a curve that is characterized by a single yield at the beginning followed by necking and a long strain hardening with a slight increase in stress during polymer deformation, which ends with a fracture at around 300% strain. This behavior was also observed in the tensile tests under water conditions (Figure 4b). In the case of PBS, its mechanical behavior is a little more particular and unique. First, an initial yield is observed that is followed by a necking and a strain hardening of the material. Subsequently, a second yield and necking appear around 80% strain, followed by a long strain hardening before ultimate failure at 220% strain. This was also noted for the PBS/PBAT nanocomposites, which have a curve shape

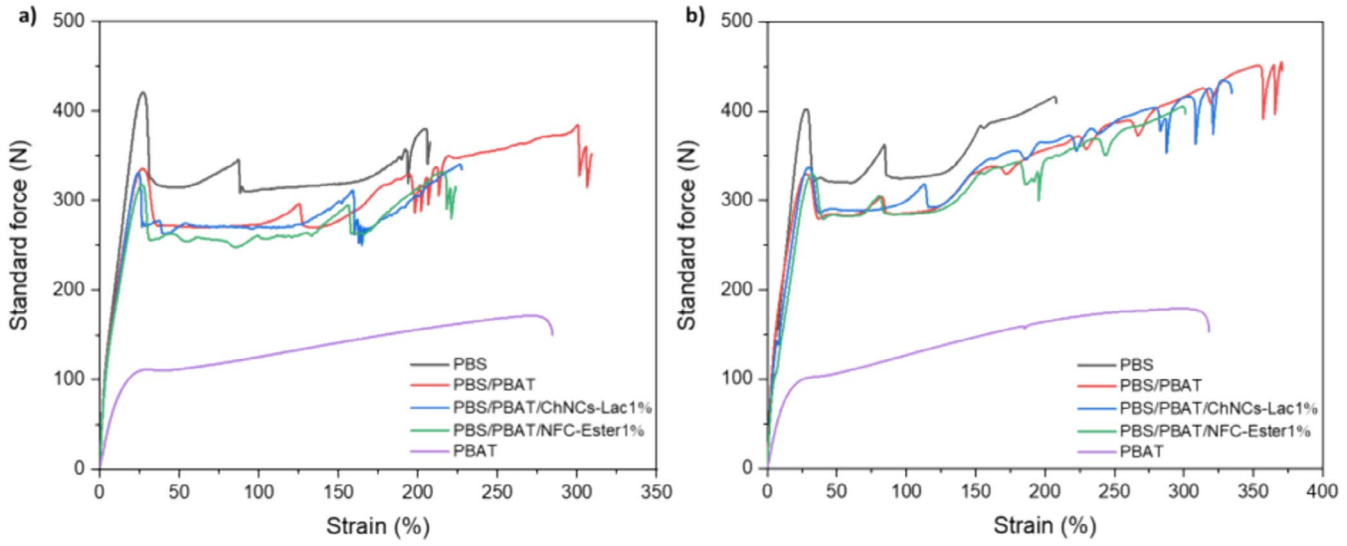


**FIGURE 4** | Tensile stress–strain curves of PBS, PBAT, PBS/PBAT, PBS/PBAT/ChNCs—Lac$_{1\%}$ and PBS/PBAT/NFC—Ester$_{1\%}$ under (a) air and (b) water conditions. [Color figure can be viewed at wileyonlinelibrary.com]

comparable to PBS. The second yield shifts toward approximately 120% strain for PBS/PBAT and toward 150% strain for PBS/PBAT/ChNCs—$Lac_{1\%}$ and PBS/PBAT/NFC—$Ester_{1\%}$. Indeed, it is also noticeable that the failure stress of PBS/PBAT nanocomposites was higher than the initial yield stress usually accompanied by strain-induced crystallization, which would have aligned the crystallites in the direction of the strain [39]. The double yielding and necking phenomena have been explained by several authors by the fact that PBS crystallizes in two different crystal structures, the α and β forms, which appear under various conditions. For example, the α form is more general and appears when PBS is crystallized from the melt, while the β form is observed under a certain level of mechanical stress [36]. Liu et al. as well as Ichikawa and Mizukoshi have demonstrated the relationship between the crystal structure transition of PBS, as revealed by XRD analysis, and the mechanical behavior variations observed on its traction tests curves [40, 41]. Secondly, a unique stress oscillation phenomenon is observed which causes a cycle of stress drop and recovery. This behavior is more pronounced in the case of PBS/PBAT nanocomposites. Wan et al. reported the same behavior for compression-molded PBS samples drawn at a lower rate under 50 mm $min^{-1}$ and also at a rate of 10 mm $min^{-1}$ under different temperatures [42]. Their study presents a clear explanation for the occurrence of these self-stress necking oscillations on the tensile curves, which can be attributed to the local increase in temperature at the neck front of the samples, the crystallization induced by the orientation of the polymer chains or to the formation of cracks and micro-cavities which were observed on their drawn samples [42]. These cracks and micro-cavities were noticed in our PBS and PBS/PBAT nanocomposite drawn samples. The tensile tests curves in water conditions (Figure 4b) of neat polymers and their blends show almost the same behavior as in air with some changes in the second yield for the PBS/PBAT and PBS/PBAT/NFC—$Ester_{1\%}$ blends, which appear in the same strain as PBS, while the second yield of PBS/PBAT/ChNCs—$Lac_{1\%}$ has shifted to 120% compared to PBS which remains at 80% strain. The stress oscillation phenomenon is absent in the case of PBS, contrary to the PBS/PBAT blend and its nanocomposites where it appears periodically until the ultimate failure of the samples.

Based on these tensile test behaviors, the variation of Young's modulus and elongation at break of the nanocomposites were also investigated under air and water conditions using screw-action manual grips (Figure 5). Firstly, both PBS and PBAT

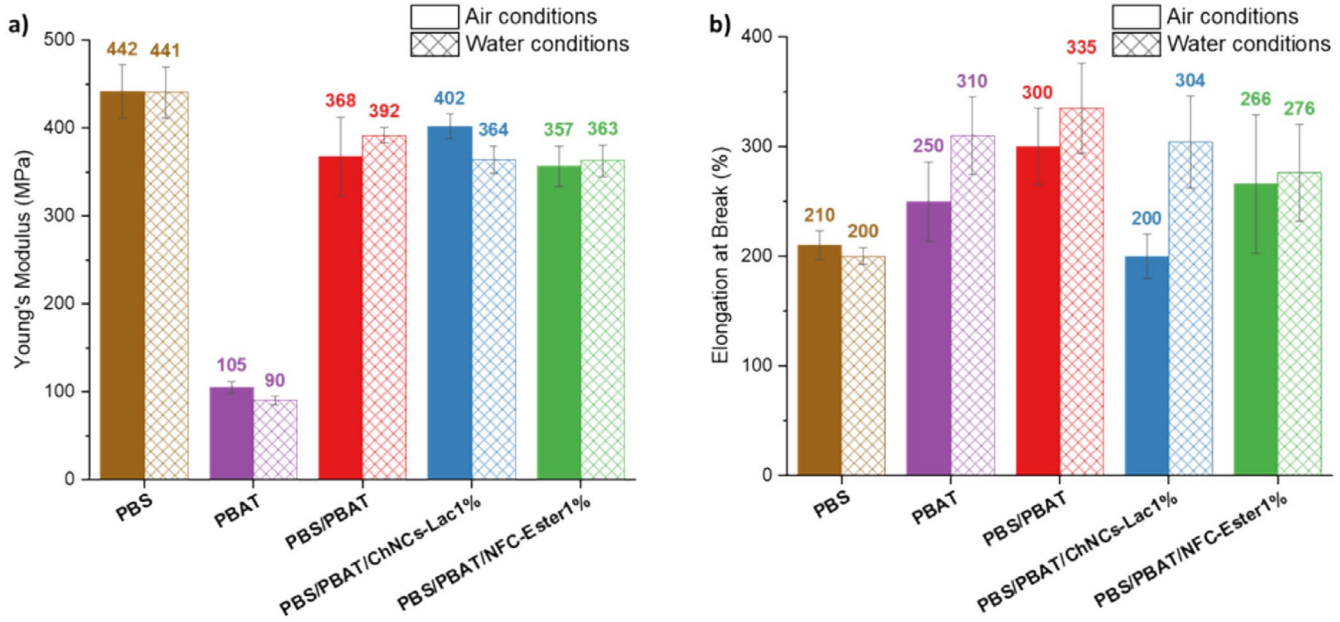


**FIGURE 5** | Comparing tensile test results of PBS/PBAT nanocomposites in air and water conditions. [Color figure can be viewed at wileyonlinelibrary.com]

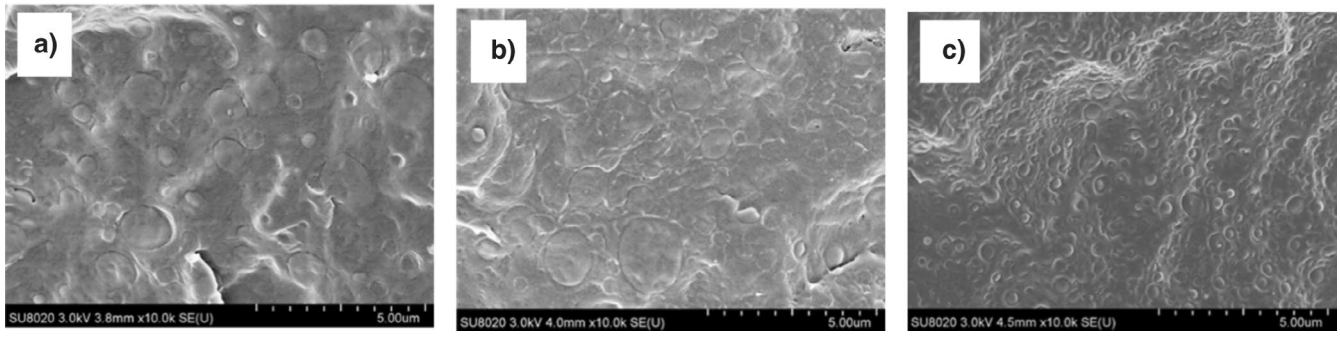


**FIGURE 6** | SEM analysis of (a) PBS/PBAT, (b) PBS/PBAT/ChNCs—$Lac_{1\%}$, and (c) PBS/PBAT/NFC—$Ester_{1\%}$.

were tested to evaluate the impact of water penetration into neat polymer. Regarding PBS, considering the standard deviation of the measurements, the mechanical properties were not influenced by the presence of water. The presence of water in PBAT also led to a similar Young's modulus but an increased elongation at break by 24%–that is, 250% versus 310%, before and after immersion, respectively. It is obvious that the PBS/PBAT blend also increases both Young's modulus (+6%) and elongation at break (+11%) in water conditions. These results relate to those found in the literature, which demonstrate an improvement of the mechanical properties of PBS/PBAT monofilaments, notably in elongation at break, when used for the first time in water [17, 43]. In the case of PBS/PBAT/NFC—$Ester_{1\%}$, considering the standard deviation of the measurements, both Young's modulus and elongation at break remain constant in water conditions. Thus, the PBS/PBAT/ChNCs—$Lac_{1\%}$ shows a slight decrease in Young's modulus (−10%) from 402 in air conditions to 364 MPa in water and a significant increase in elongation at break value (+52%) from 200% in air conditions to 304% in water. However, these values remain lower than those of PBS/PBAT blend and do not reveal a significant improvement of the mechanical properties of the blend by the addition of nanochitin and nanocellulose fillers. In fact, many factors can affect the mechanical behavior of these nanocomposites. The presence of water generally acts as a plasticizer for many polymers, including PBS and PBAT, which reduces Young's modulus values, indicating a decrease in the stiffness of the materials. This was particularly evident for PBAT and PBS/PBAT/ChNCs—$Lac_{1\%}$. It also leads to an increase in elongation at break values that indicate an enhanced ductility that was shown in particular for PBS/PBAT, PBS/PBAT/ChNCs—$Lac_{1\%}$, and PBS/PBAT/NFC—$Ester_{1\%}$.

The mechanical behavior of the nanocomposites can also be affected by the morphology of nanofillers in the polymer matrix, such as type and shape, dispersion, distribution, and mass fraction of nanofillers. The chemical and physical interactions between the polymeric matrix and nanofillers are likewise important and can result in changes in the crystallinity of the material, which affects mechanical properties [44]. To investigate these factors and their relationship with the mechanical behavior of the nanocomposites, supplementary analyses on the morphological properties of PBS/PBAT nanocomposites will be conducted.

## 3.5 | Scanning Electron Microscopy Analysis (SEM)

To further understand the thermal and mechanical properties of the PBS/PBAT blend before and after the addition of ChNCs—Lac and NFC—Ester, scanning electron microscopy (SEM) was used to examine their morphology. Figure 6a shows that the PBS/PBAT blend is characterized by a homogenous surface, which is representative of the PBS matrix, with the appearance of large nodules, which is representative of the PBAT matrix [45]. It is also observed that the PBAT is dispersed uniformly in the major matrix (PBS), which may indicate a compatibilization of the two polymers. This was also observed in the tensile test results, where the mechanical properties of the PBS/PBAT blend were improved compared to the neat polymers. In fact, this morphological behavior of PBS/PBAT was mentioned in a study by Muthuraj et al. who used the same extrusion conditions on different fractions of the PBS/PBAT blend and explained this by a transesterification reaction between the PBS and PBAT polymers. This reaction leads to a compatibilization of the two polymers, and as a result, an improvement in the mechanical properties [23, 46]. Through the incorporation of ChNCs—$Lac_{1\%}$ with the blend (Figure 6b), we noticed that some nodules became smaller and more closely linked. Additionally, in some areas, the PBAT nodules started to slightly merge with the PBS matrix and appeared as a one homogeneous matrix. This is potentially due to the increase in the transesterification reaction rate between the two polymers by adding the ChNCs—Lac. In contrast, the PBS/PBAT/NFC—$Ester_{1\%}$ blend (Figure 6c) exhibited fewer and more persistent nodules across the majority matrix compared to the two other blends. However, a separation phase between the two matrices was also noticed. Similar results for the PBS/NFC nanocomposites were reported in the literature [47]. Thus, these observations allow us to say that the nanofillers have a good dispersion in the PBS/PBAT blend, which is shown in the morphology of the blend before and after adding nanofillers, especially for the PBS/PBAT/ChNCs—$Lac_{1\%}$ blend with more interaction with PBS. In order to investigate the impact of the presence of well-dispersed nanofiller, weathering tests were conducted with ChNCs—$Lac_{1\%}$.

## 3.6 | Weathering Tests

### 3.6.1 | Mechanical Properties After Weathering Tests

Tensile tests were carried out under water conditions to comprehend the mechanical behavior of the nanocomposites under controlled and accelerated weathering conditions. The weathering tests under accelerated conditions are usually used to study the degradation behavior of the polymers and their physico-chemical properties changes [28, 48]. PBS, PBS/PBAT, and PBS/PBAT/ChNCs—$Lac_{1\%}$ were exposed to humidity and a temperature of 75°C for 8 days. The tensile curves of the three nanocomposites after 2, 4, and 8 days of weathering are presented in Figure 7. From these curves, we can already observe that the three nanocomposites had a significant loss of mechanical properties starting from the 2nd days of weathering, which became more significant with time. This is also confirmed by the variations in Young's modulus and elongation at break values presented in Figure 8. These significantly decreased after 2 days of weathering for the three nanocomposites, especially for PBS/PBAT/ChNCs—$Lac_{1\%}$, with a loss of −40% for Young's modulus and 74% for elongation at break, compared to PBS/PBAT, which had a loss of −33% for Young's modulus and−33% for elongation at break, and the neat PBS with a loss of −12% for Young's modulus and −76% for elongation at break. This decrease is caused by the degradation of the polymer due to a hydrolysis reaction that is accelerated by a high temperature and humidity. This behavior was also observed by several authors, such as Muthuraj et al., who studied the hydrolytic degradation of the PBS/PBAT blend under different controlled weathering conditions [49, 50].

Plasticization is another phenomenon that can occur in nanocomposites and for the majority of polymers [51, 52]. Plasticization is caused by water absorption in the polymer matrix, which acts

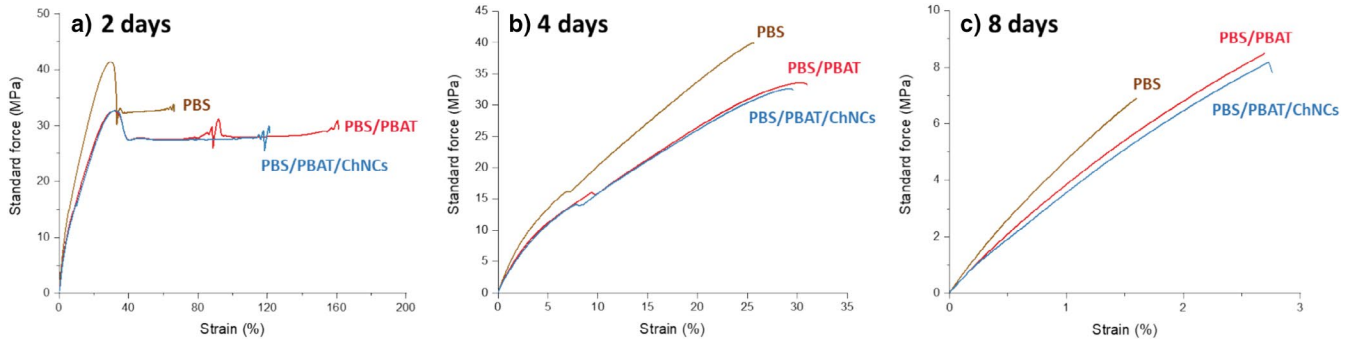


**FIGURE 7** | Tensile test curves in water conditions of PBS, PBS/PBAT, and PBS/PBAT/ChNCs—$Lac_{1\%}$ after (a) 2, (b) 4, and (c) 8 days of weathering tests. [Color figure can be viewed at wileyonlinelibrary.com]

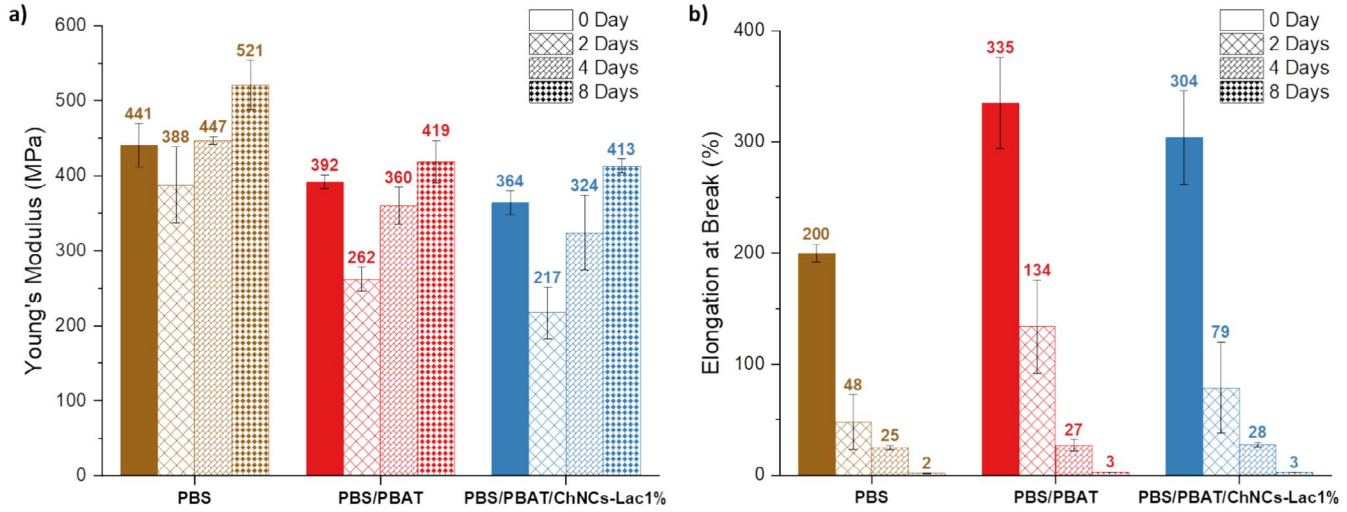


**FIGURE 8** | Comparing tensile properties of PBS, PBS/PBAT, and PBS/PBAT/ChNCs—$Lac_{1\%}$ in different weathering time. [Color figure can be viewed at wileyonlinelibrary.com]

as a plasticizer and reduces its stiffness. This is confirmed by a decrease in Young's modulus for the three nanocomposites. Thus, water tends to penetrate the amorphous regions of a polymer more than the crystalline regions, increasing the hydrolysis reaction in the amorphous regions and leading to rapid degradation of these regions. This was noticed in the two nanocomposites PBS/PBAT and PBS/PBAT/ChNCs—$Lac_{1\%}$, which had a greater loss of mechanical properties compared to neat PBS. This is due to the presence of PBAT, which is characterized by low crystallinity and, consequently, a high rate of amorphous regions in its polymeric structure. This induces water penetration and higher degradation compared to neat PBS.

The 4th and 8th day of weathering showed a significant increase in Young's modulus with a continued decrease in elongation at break for the three nanocomposites, particularly for the PBS/PBAT/ChNCs—$Lac_{1\%}$ blend. A significant increase in Young's modulus is generally attributed to an increase in the crystallinity rate, which is the result of the creation of hydroxyl and carboxylic acid end groups generated by the scission of the ester chains of the polymer. This behavior is mainly related to PBS degradation since it is the majority matrix of the three nanocomposites. In fact, PBS is very sensitive to moisture, so a continuous exposure to a humid environment reduces its toughness, which decreases its elongation at break. This was demonstrated by Muthuraj et al. when they compared the variation in elongation at break of PBS with polypropylene (PP) over 6 days of weathering. This result shows that PBS loses its toughness more quickly compared to PP [50].

The hydrolysis reaction proceeds rapidly for PBS under controlled conditions, such as high temperature and moisture, showing an acceleration of polymer degradation. While the addition of PBAT in the matrix firstly contributes to slightly delaying this degradation, especially after 2 days of weathering. However, in the 4th and 8th days of weathering, the degradation is more accelerated with the presence of PBAT due to the higher absorption of water by the amorphous regions of this polymer [53, 54].

On the other hand, the addition of nanochitins to the PBS/PBAT polymer matrix enhances its degradation, resulting in lower values of Young's modulus and elongation at break compared to those of the PBS/PBAT blend over weathering time.

### 3.6.2 | Morphological Properties After Weathering Tests

To investigate the considerable loss in mechanical properties during weathering tests for the three nanocomposites, SEM

measurements were conducted on the nanocomposites at 0 and 8 days of weathering. Figure 9 presents the SEM micrographs taken from the surface of the nanocomposites before and after 8 days of weathering. Apparently, the PBS/PBAT and PBS/PBAT/ChNCs—$Lac_{1\%}$ undergo significant changes in their morphology. This is observed by scratches on the surface of the nanocomposites after 8 days of weathering, while these scratches are not visible on the surface of the non-weathered samples. The PBS/PBAT/ChNCs—$Lac_{1\%}$ blend reveals more pronounced surface abrasion compared to PBS/PBAT, which is supported by the mechanical tests showing that the addition of nanochitins enhances the degradation of the blend (See white circle into Figure 9).

For the PBS, no changes were observed on the surface of the polymer after 8 days exposed to humidity and 75°C, which is inconsistent with the tensile test results that showed a significant loss of mechanical properties after 8 days of weathering. Indeed, SEM analyses on the cross section of the PBS before and after 8 days of weathering were carried out, and the SEM micrographs are presented in Figure 10. The weathered PBS shows scratches and voids in its structure compared to that of the non-weathered PBS. The PBS, like the majority of polyesters, predominantly undergoes degradation by surface abrasion; however, a biodegradation in the bulk stage sometimes occurs, which can be inferred through molecular weight reduction. This was also reported in a study on the hydrolytic degradation of polylactic acid (PLA) [55].

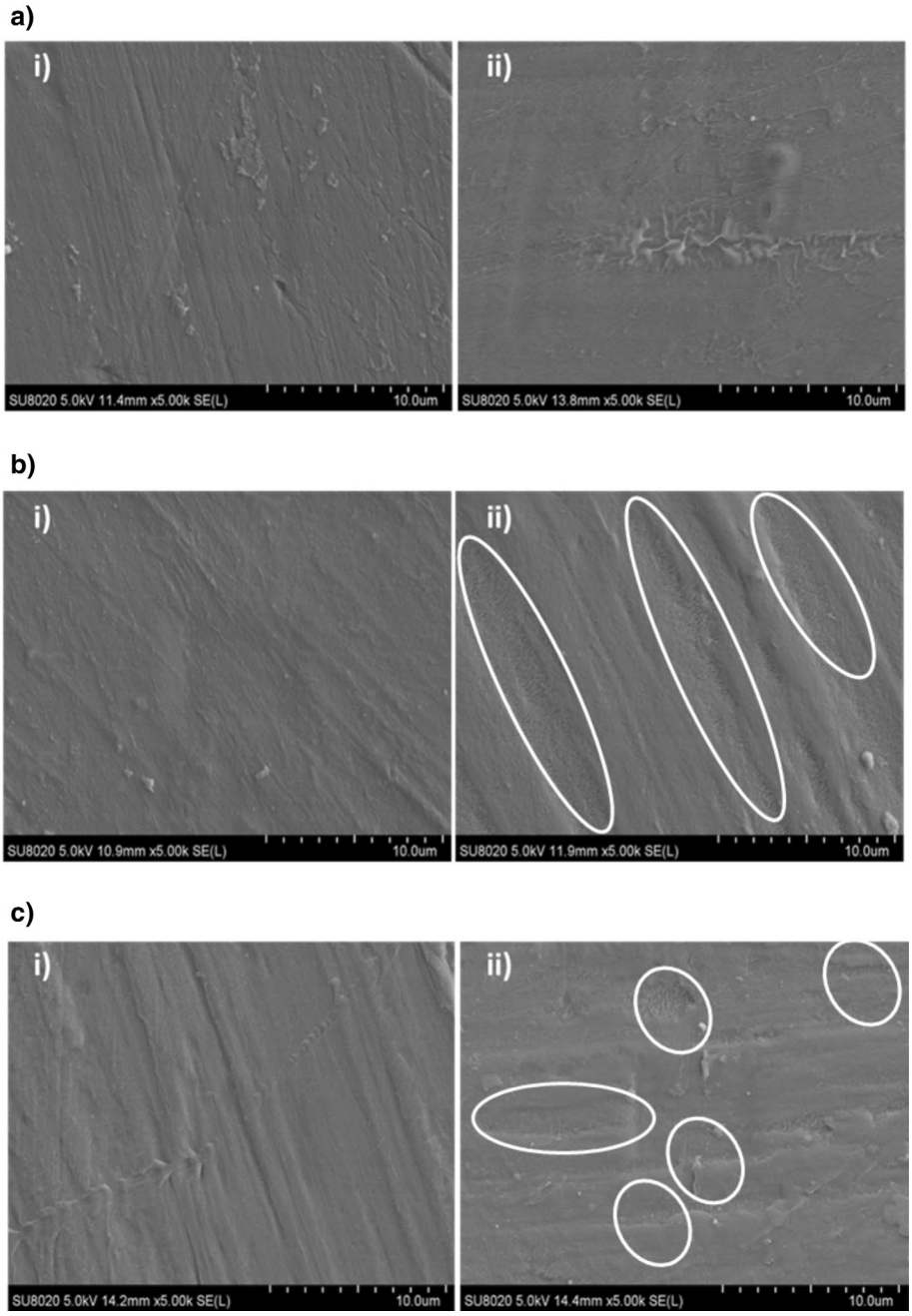


**FIGURE 9** | SEM surface micrographs of (a) PBS, (b) PBS/PBAT, and (c) PBS/PBAT/ChNCs—$Lac_{1\%}$ non-weathered (i samples) and after 8 days of weathering (ii samples).

### 3.6.3 | Thermal Properties After Weathering Tests

The weathering tests of the three nanocomposites revealed a significant loss of mechanical properties, allowing changes in the crystal structure of the polymers, as well as their thermal characteristics, to be estimated. DSC analysis was carried out for the three nanocomposites on days 0, 2, 4, and 8 of weathering. The thermograms of the cooling cycle and the second heating cycle are presented in Figure 11. Only the curves of the non-weathered nanocomposites and those obtained after 8 days of weathering were selected and presented in the graphs, since there were no significant modifications observed in the curves of the 2nd and 4th days of weathering. The values of the thermal properties of the nanocomposites are presented in Table 4, and the variations of the values of $T_c$, $\Delta H_c$, $\Delta H_m$, and $\chi_c$ as a function of the weathering time are presented in the graphs of Figure 12.

From the cooling cycle curves presented in Figure 11a, we can observe a shift of the crystallization peaks toward lower $T_c$ values for all the nanocomposites after the 8th day of weathering compared to the non-weathered samples. This is also demonstrated by the $T_c$ values (Table 4) which started to decrease from the 2nd day of weathering. This decrease is more significant for the PBS/PBAT and PBS/PBAT/ChNCs—$Lac_{1\%}$ blends. $\Delta H_c$ decreases after 2 days of weathering and then slightly increases (Table 4, Figure 12b) because the amorphous part is degraded; then the relative crystallinity increases.

Looking at the curves of the second heating cycle shown in Figure 11b, we can see the presence of an endothermic melting peak and an exothermic peak, related to the PBS matrix, as aforementioned, in all the non-weathered samples. After 8 days of weathering, it is clearly shown that the exothermic peak, related to the cold recrystallization, shifts to lower temperatures in all three nanocomposites. After the cold recrystallization, and before the second melting peak, we observe the appearance of a new melting peak, which is more pronounced in PBS compared to PBS/PBAT and PBS/PBAT/ChNCs-$Lac_{1\%}$. This melting peak was mentioned in the study of Wang et al. and was observed in PBS samples crystallizing at $T_{cc} \geq 70°C$ [38]. The melting enthalpies $\Delta H_m$ and the crystallinity rate $\chi_c$ increase significantly during the degradation of all samples, which is clearly observed in the variation graphs of Figure 12c,d. These variations are explained by the formation of short molecular chains during the hydrolysis of the polymers that lead to the phenomenon of chemicrystallization. This phenomenon creates chemical modifications in the polymer structure which, during

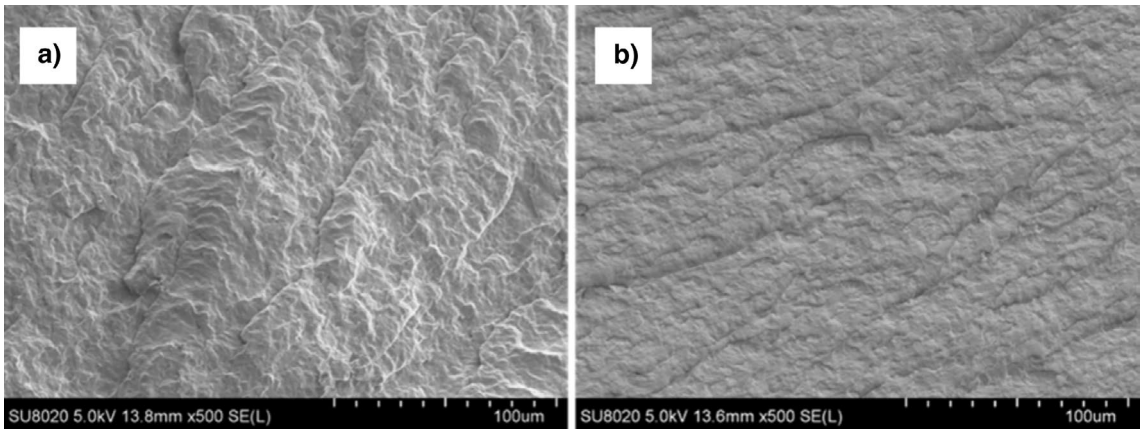


**FIGURE 10** | SEM micrographs of a cross-section of the PBS (a) before weathering and (b) after 8 days of weathering.

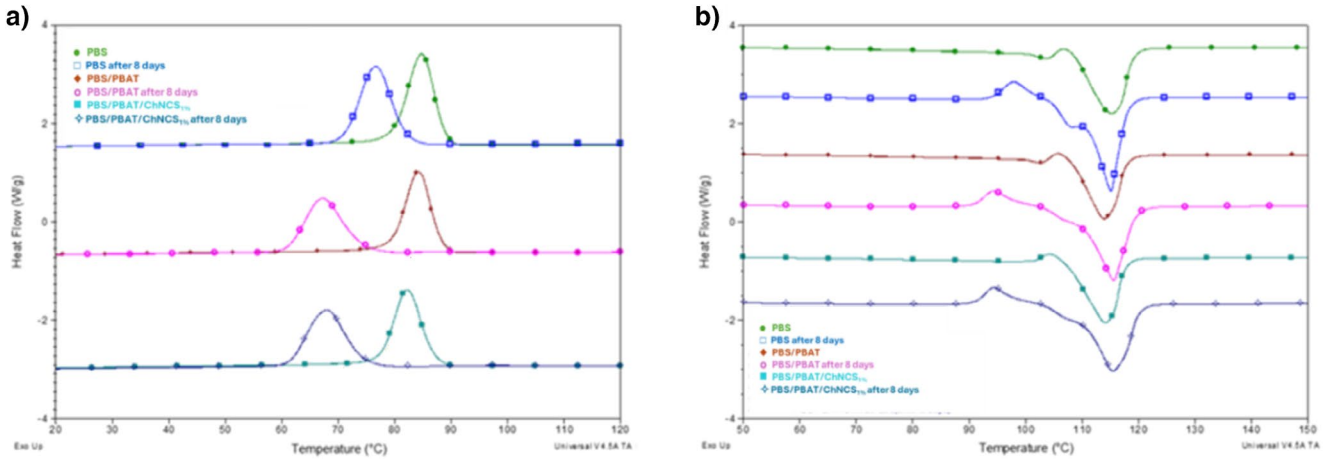


**FIGURE 11** | DSC thermograms of PBS, PBS/PBAT, and PBS/PBAT/ChNCs—$Lac_{1\%}$ before and after 8 days of weathering on (a) the cooling run and (b) the second heating run. [Color figure can be viewed at wileyonlinelibrary.com]

**TABLE 4** | DSC results of the cooling and second heating cycles of the samples used in weathering tests.

| Samples | Cooling cycle | | Second heating cycle | | | |
|---|---|---|---|---|---|---|
| | $T_c$ (°C) | $\Delta H_c$ (J g$^{-1}$ $_{PBS}$) | $T_g$ (°C) | $T_m$ (°C) | $\Delta H_m$ (J g$^{-1}$ $_{PBS}$) | $\chi_{c\ PBS}$ (%) |
| PBS | 85 | 68 | −31 | 115 | 55 | 28 |
| PBS (after 2 days) | 76 | 64 | −32 | 119 | 73 | 37 |
| PBS (after 4 days) | 75 | 68 | −30 | 117 | 100 | 50 |
| PBS (after 8 days) | 77 | 67 | −29 | 115 | 92 | 46 |
| PBS/PBAT | 84 | 62 | −32 | 114 | 50 | 25 |
| PBS/PBAT (after 2 days) | 73 | 53 | −31 | 116 | 67 | 34 |
| PBS/PBAT (after 4 days) | 70 | 54 | −31 | 115 | 77 | 39 |
| PBS/PBAT (after 8 days) | 67 | 55 | −32 | 116 | 86 | 43 |
| PBS/PBAT/ChNCs—Lac | 82 | 60 | −29 | 114 | 55 | 28 |
| PBS/PBAT/ChNCs—Lac (after 2 days) | 75 | 54 | −31 | 115 | 67 | 34 |
| PBS/PBAT/ChNCs—Lac (after 4 days) | 70 | 56 | −30 | 115 | 79 | 40 |
| PBS/PBAT/ChNCs—Lac (after 8 days) | 68 | 57 | −32 | 115 | 88 | 44 |

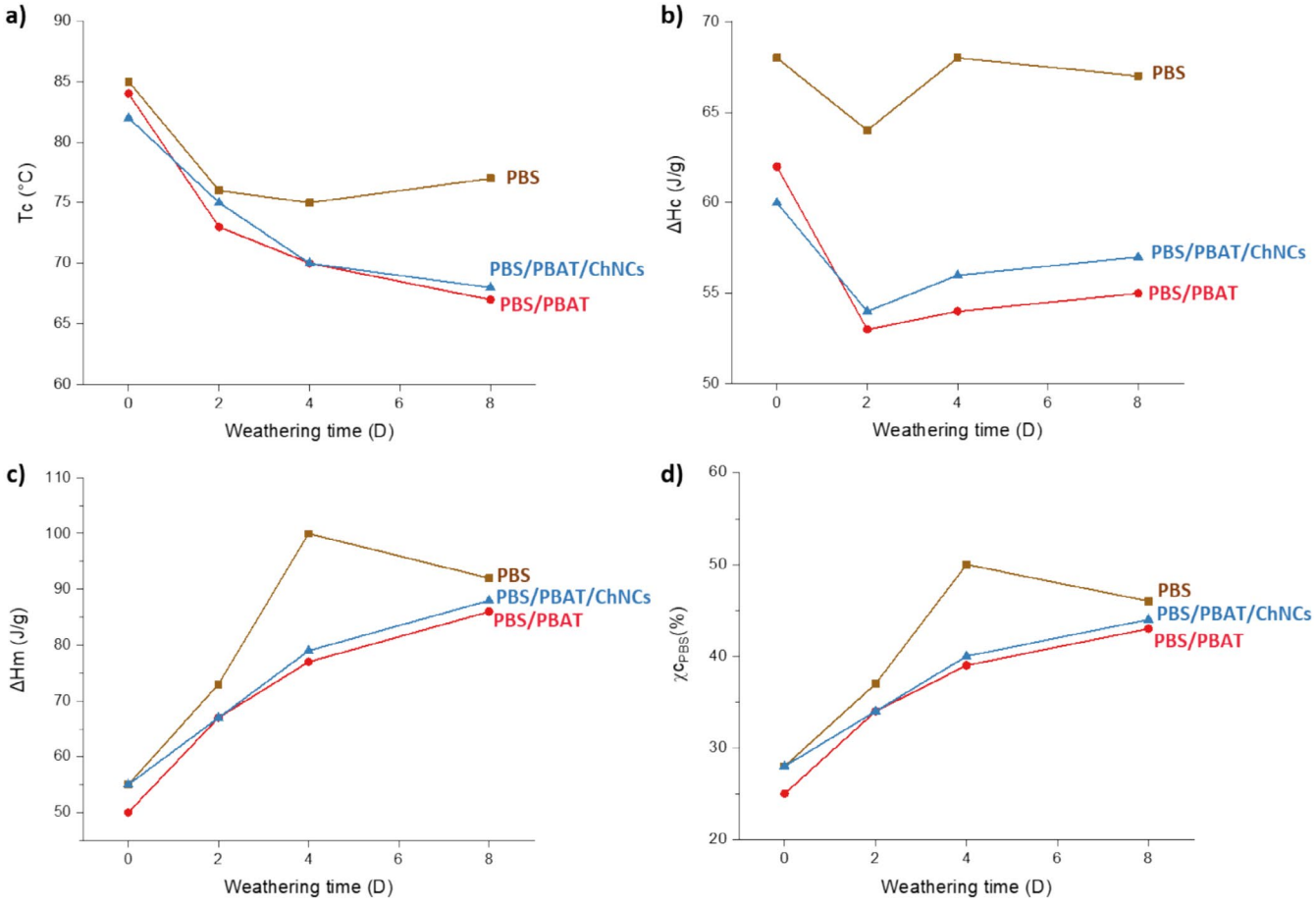


**FIGURE 12** | Variation curves in the cooling cycle (a) $T_c$ and 2nd heating cycle presented by (b) $T_g$, (c) $\Delta H_m$, and (d) $\chi_c$. [Color figure can be viewed at wileyonlinelibrary.com]

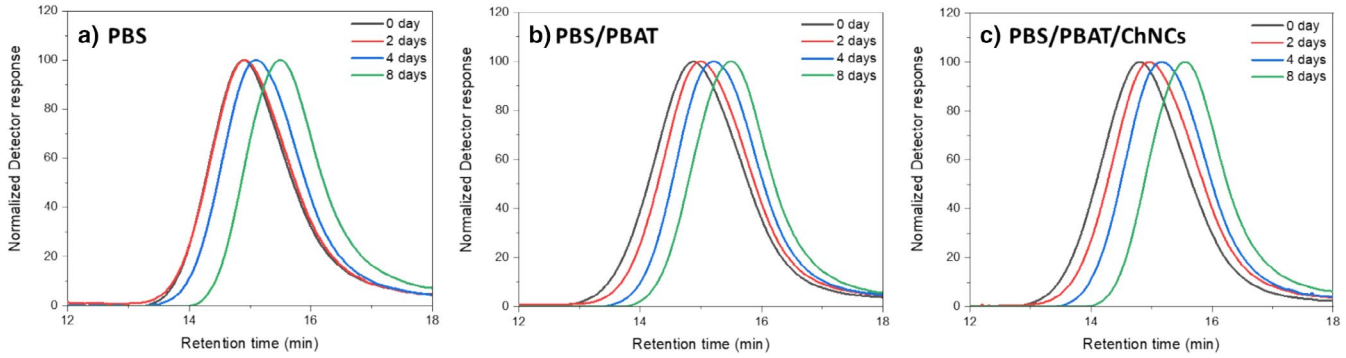


**FIGURE 13** | Variation of GPC chromatograms of (a) PBS, (b) PBS/PBAT, and (c) PBS/PBAT/ChNCs during weathering tests. [Color figure can be viewed at wileyonlinelibrary.com]

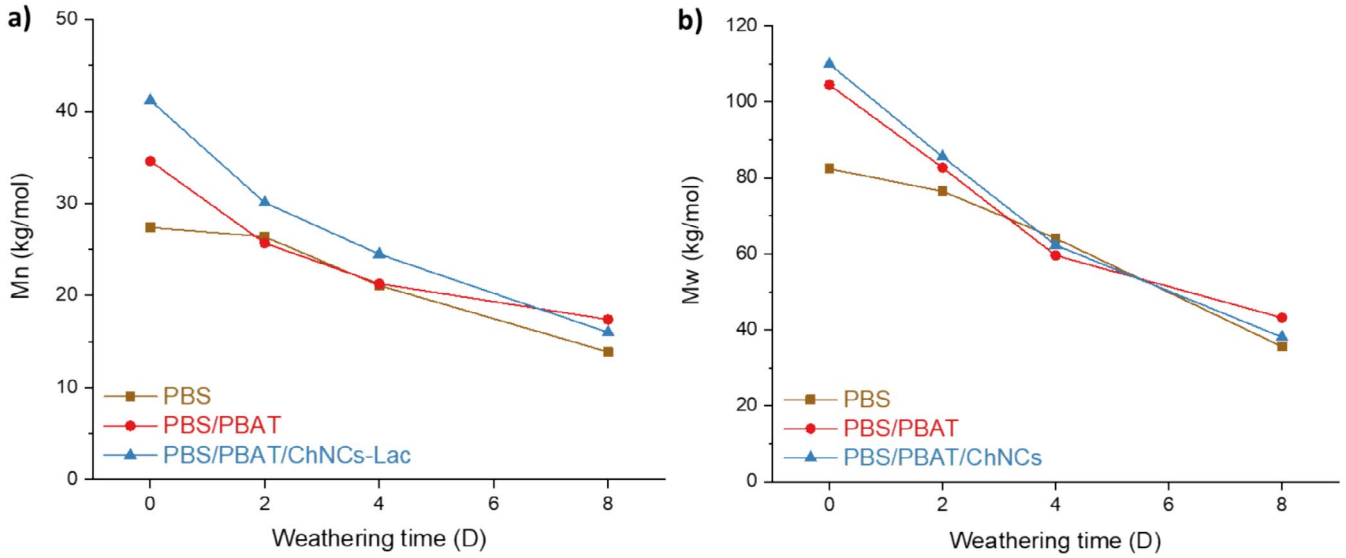


**FIGURE 14** | Variation of (a) $M_n$ and (b) $M_w$ by weathering time for the PBS, PBS/PBAT, and PBS/PBAT/ChNCs used in weathering tests. [Color figure can be viewed at wileyonlinelibrary.com]

its crystallization, can affect the size, thickness, or the distribution of the crystals formed in the polymeric matrix.

### 3.6.4 | SEC Measurement After Weathering Tests

Chemical characterization was carried out by SEC analysis in order to identify physicochemical changes in the three nanocomposites used in the weathering tests and to corroborate the mechanical and thermal results of the samples. The GPC chromatograms of PBS, PBS/PBAT, and PBS/PBAT/ChNCs during weathering tests are presented in Figure 13, and the variation of $M_n$ and $M_w$ of the three nanocomposites, as a function of weathering time, is shown in Figure 14.

It is clearly noted that the molecular weight significantly decreased throughout the entire weathering period for the three nanocomposites. The PBS/PBAT/ChNCs—$Lac_{1\%}$ blend had a decrease of 61% in $M_n$ and 56% in $M_w$, which is higher compared to PBS/PBAT, with a loss of 38% in $M_n$ and 43% in $M_w$, and PBS with a decrease of 50% in $M_n$ and 22% in $M_w$. These results show that the PBS/PBAT/ChNCs—$Lac_{1\%}$ has a higher degradation rate compared to the other nanocomposites, which corresponds with the results of the mechanical and thermal analysis.

A comparison with similar studies allows to highlight the interest of our nanofiller strategy developed in this study. For instance, Fu et al. reported reinforcement effects with nanochitins, which aligns with our findings, where we observed an interesting effect on foam process of PBS reinforced with chitin nanofillers [35]. Similarly, Salaberria et al. demonstrated the positive impact of functionalized nanocelluloses on enhancing crystallinity and mechanical performance of PLA [32], which is consistent with our results, particularly with the PBS/PBAT/NFC—$Ester_{1\%}$ nanocomposite. These studies further validate the potential of nanochitin and nanocellulose as effective nanofillers for improving the mechanical properties of biodegradable polymers.

## 4 | Conclusion

This study aimed to investigate and understand the mechanical and morphological behavior of the PBS/PBAT polymer

blend, which is currently being explored as a replacement for conventional nylon fishing nets, before and after incorporating nanochitin and nanocellulose fillers. An initial mechanical characterization through tensile tests in air conditions was performed on nanocomposites prepared with various functionalizations of nanochitin and nanocellulose fillers. This allowed for the selection of the nanocomposites that demonstrated the most significant mechanical reinforcement when blended with PBS/PBAT. Among these, PBS/PBAT/ChNCs—$Lac_{1\%}$ and PBS/PBAT/NFC—$Ester_{1\%}$ exhibited a notable enhancement in mechanical properties compared to the other nanocomposites. This improvement suggests a good dispersion of the nanofillers within the PBS/PBAT blend, as further confirmed by SEM analysis, which revealed favorable morphology both before and after the addition of nanofillers, particularly for the PBS/PBAT/ChNCs—$Lac_{1\%}$ blend with enhanced interaction with PBS. Additionally, DSC and GPC results corroborated these mechanical and morphological findings. However, tensile tests under water conditions did not indicate a significant improvement in the mechanical properties of the PBS/PBAT nanocomposites compared to the unmodified PBS/PBAT blend.

The degradation behavior of PBS, PBS/PBAT, and PBS/PBAT/ChNCs—$Lac_{1\%}$ was also studied under accelerated degradation conditions. All three exhibited hydrolytic degradation starting from the 2nd day of weathering, with PBS degrading at a higher rate. Although the inclusion of PBAT in the matrix initially contributed to a slight delay in degradation before the 4th day of weathering, the degradation rate then accelerated, particularly for PBS/PBAT/ChNCs—$Lac_{1\%}$, which displayed a lower Young's modulus and elongation at break compared to the PBS/PBAT blend over time. Morphological analysis revealed more pronounced surface abrasion in PBS/PBAT/ChNCs—$Lac_{1\%}$ compared to PBS/PBAT, which was consistent with the mechanical testing results, indicating that the addition of nanochitin accelerates the blend's degradation. This was further supported by the greater decrease in molecular weight observed via GPC analysis and variations in thermal properties noted in DSC analysis. These findings position chitin and cellulose nanofillers as promising additives for PBS/PBAT blends; however, further research should aim to enhance mechanical performance under water conditions by experimenting with new formulations and testing monofilaments made from these nanocomposites. In addition, it is crucial to conduct durability tests under repeated environmental engineering conditions, such as cyclic exposure to marine water and varying mechanical stresses, to simulate real-world fishing scenarios. This would provide a more comprehensive understanding of the long-term performance and reliability of these materials. Moreover, in line with a balanced approach, future publications will address the ecotoxicological impact of these nanocomposites following their degradation into microplastics within marine environments.

### Author Contributions

**Yousra Nait Hamou:** investigation (equal), methodology (equal), writing – original draft (lead). **Samira Benali:** conceptualization (equal), funding acquisition (lead), investigation (equal), methodology (equal), supervision (equal), writing – original draft (supporting), writing – review and editing (lead). **Mostapha Benomar:** conceptualization (supporting), funding acquisition (equal), writing – review and editing (supporting). **Sandro Gennen:** resources (equal). **Jean-Michel Thomassin:** resources (lead). **Job Tchoumtchoua:** resources (equal). **Hassan Er-Raioui:** supervision (equal), validation (equal). **Jean-Marie Raquez:** conceptualization (equal), investigation (equal), methodology (equal), supervision (lead), validation (equal), writing – review and editing (equal).

### Acknowledgments

This work is supported by "Académie de Recherche et d'Enseignement supérieur, (ARES)" in the framework of Research & Development Project (2022–2027 Program) between Belgium and European Regional Development Fund (ERDF-FEDER) for general support in the frame of UP_PLASTICS portofolio. Jean-Marie Raquez is an F.R.S.–FNRS Research Associate.

### Conflicts of Interest

The authors declare no conflicts of interest.

### Data Availability Statement

All source data available.

### References

1. E. Brivio, I. Petsa, and T. Mc Phie, *Single-Use Plastics: New EU Rules to Reduce Marine Litter* (European Commission, 2018).

2. M. Sullivan, S. Evert, P. Straub, et al., "Identification, Recovery, and Impact of Ghost Fishing Gear in the Mullica River-Great Bay Estuary (New Jersey, USA): Stakeholder-Driven Restoration for Smaller-Scale Systems," *Marine Pollution Bulletin* 138 (2019): 37–48.

3. M. Oleksy, K. Dynarowicz, and D. Aebisher, "Advances in Biodegradable Polymers and Biomaterials for Medical Applications," *Molecules* 28, no. 1 (2023): 6213–6231.

4. A. Samir, F. H. Ashour, A. A. A. Hakim, and M. Bassyouni, "Recent Advances in Biodegradable Polymers for Sustainable Applications," *NPJ Materials Degradation* 6, no. 1 (2022): 68, https://doi.org/10.1038/s41529-022-00277-7.

5. M. Yu, Y. Tang, M. Min, et al., "Comparison of Physical Properties and Fishing Performance Between Biodegradable PLA and Conventional PA Trammel Nets in Grey Mullet (Mugil Cephalus) and Red-Lip Mullet (Liza Haematocheila) Fishery," *Marine Pollution Bulletin* 195 (2023): 115545.

6. A. Delacuvellerie, S. Benali, V. Cyriaque, et al., "Microbial Biofilm Composition and Polymer Degradation of Compostable and Non-Compostable Plastics Immersed in the Marine Environment," *Journal of Hazardous Materials* 419 (2021): 126526.

7. S.-W. Park, J.-H. Bae, J.-H. Lim, et al., "Development and Physical Properties on the Monofilament for Gill Nets and Traps Using Biodegradable Aliphatic Polybutylene Succinate Resin," *Bulletin of the Korean Society of Fisheries Technology* 43 (2007): 281–290.

8. PTT MCC Biochem, "BioPBS Trademark", https://www.pttmcc.com/about-us.

9. O. Platnieks, S. Gaidukovs, V. Kumar Thakur, A. Barkane, and S. Beluns, "Bio-Based Poly (Butylene Succinate): Recent Progress, Challenges and Future Opportunities," *European Polymer Journal* 161 (2021): 110855.

10. C. C. Satam, M. Daub, and M. J. Realff, "Techno-Economic Analysis of 1,4-Butanediol Production by a Single-Step Bioconversion Process," *Biofuels, Bioproducts and Biorefining* 13, no. 5 (2019): 1261–1273, https://doi.org/10.1002/bbb.2016.

11. G. X. Wang, D. Huang, J. H. Ji, C. Völker, and F. R. Wurm, "Seawater-Degradable Polymers—Fighting the Marine Plastic Pollution," *Advanced Science* 8, no. 1 (2021): 2001121.

12. A. Nakayama, N. Yamano, and N. Kawasaki, "Biodegradation in Seawater of Aliphatic Polyesters," *Polymer Degradation and Stability* 166 (2019): 290–299.

13. J. Kim, S. Park, S. Jung, et al., "Biodegradation Behavior of Polybutylene Succinate (PBS) Fishing Gear in Marine Sedimentary Environments for Ghost Fishing Prevention," *Polymer Degradation and Stability* 216 (2023): 110490.

14. S.-W. Park, C.-D. Park, J.-H. Bae, and J.-H. Lim, "Catching Efficiency and Development of the Biodegradable Monofilament Gill Net for Snow Crab, Chionoecetes Opilio," *Journal of the Korean Society of Fisheries and Ocean Technology* (2007): 28–37.

15. S.-W. Park and J.-H. Bae, "Weatherability of Biodegradable Polybutylene Succinate(PBS) Monofilaments," *Bulletin of the Korean Society of Fisheries Technology* 44 (2008): 265–272.

16. S.-W. Park, S.-H. Kim, H.-S. Choi, and H.-H. Cho, "Preparation and Physical Properties of Biodegradable Polybutylene Succinate/Polybutylene Adipate-Co-Terephthalate Blend Monofilament by Melt Spinning," *Bulletin of the Korean Society of Fisheries Technology* 46 (2010): 257–264.

17. S. Kim, P. Kim, J. Lim, H. An, and P. Suuronen, "Use of Biodegradable Driftnets to Prevent Ghost Fishing: Physical Properties and Fishing Performance for Yellow Croaker," *Animal Conservation* 19, no. 4 (2016): 309–319, https://doi.org/10.1111/acv.12256.

18. J. Jacquin, N. Callac, J. Cheng, et al., "Microbial Diversity and Activity During the Biodegradation in Seawater of Various Substitutes to Conventional Plastic Cotton Swab Sticks," *Frontiers in Microbiology* 12, no. 1 (2021): 604395, https://doi.org/10.3389/fmicb.2021.604395.

19. L. Aliotta, V. Gigante, O. Acucella, F. Signori, and A. Lazzeri, "Thermal, Mechanical and Micromechanical Analysis of PLA/PBAT/POE-g-GMA Extruded Ternary Blends," *Frontiers in Materials* 7, no. 1 (2020): 130, https://doi.org/10.3389/fmats.2020.00130.

20. S. Kim, S. w. Park, and K. Lee, "Fishing Performance of Environmentally Friendly Tubular Pots Made of Biodegradable Resin (PBS/PBAT) for Catching the Conger Eel Conger Myriaster," *Fisheries Science* 80, no. 5 (2014): 887–895, https://doi.org/10.1007/s12562-014-0785-z.

21. E. Grimaldo, B. Herrmann, B. Su, et al., "Comparison of Fishing Efficiency Between Biodegradable Gillnets and Conventional Nylon Gillnets," *Fisheries Research* 213 (2019): 67–74.

22. E. Grimaldo, B. Herrmann, N. Jacques, et al., "The Effect of Long-Term Use on the Catch Efficiency of Biodegradable Gillnets," *Marine Pollution Bulletin* (2020): 111823.

23. R. Muthuraj, M. Misra, and A. K. Mohanty, "Biodegradable Poly(Butylene Succinate) and Poly(Butylene Adipate-Co-Terephthalate) Blends: Reactive Extrusion and Performance Evaluation," *Journal of Polymers and the Environment* 22 (2014): 336–349.

24. A. Mtibe, L. Hlekelele, P. E. Kleyi, et al., "Fabrication of a Polybutylene Succinate (PBS)/Polybutylene Adipate-Co-Terephthalate (PBAT)-Based Hybrid System Reinforced With Lignin and Zinc Nanoparticles for Potential Biomedical Applications," *Polymers* 14 (2022): 5065–5079.

25. H. Pulikkalparambil, D. Phothisarattana, K. Promhuad, and N. Harnkarnsujarit, "Effect of Silicon Dioxide Nanoparticle on Microstructure, Mechanical and Barrier Properties of Biodegradable PBAT/PBS Food Packaging," *Food Bioscience* 55 (2023): 103023.

26. D. Meng, J. Xie, G. I. N. Waterhouse, et al., "Biodegradable Poly(Butylene Adipate-Co-Terephthalate) Composites Reinforced With Bio-Based Nanochitin: Preparation, Enhanced Mechanical and Thermal Properties," *Journal of Applied Polymer Science* 137 (2020): 137.

27. C. Calvino, N. Macke, R. Kato, and S. J. Rowan, "Development, Processing and Applications of Bio-Sourced Cellulose Nanocrystal Composites," *Progress in Polymer Science* 103 (2020): 101221.

28. C. Kanemura, S. Nakashima, and A. Hotta, "Mechanical Properties and Chemical Structures of Biodegradable Poly(Butylene-Succinate) for Material Reprocessing," *Polymer Degradation and Stability* 97 (2012): 972–980.

29. C. Magnani, A. Idström, L. Nordstierna, et al., "Interphase Design of Cellulose Nanocrystals/Poly(Hydroxybutyrate- ran -Valerate) Bionanocomposites for Mechanical and Thermal Properties Tuning," *Biomacromolecules* 21, no. 5 (2020): 1892–1901, https://doi.org/10.1021/acs.biomac.9b01760.

30. C. Magnani, M. Fazilati, R. Kádár, et al., "Green Topochemical Esterification Effects on the Supramolecular Structure of Chitin Nanocrystals: Implications for Highly Stable Pickering Emulsions," *ACS Applied Nano Materials* 5 (2022): 4731–4743.

31. A. R. de Matos Costa, A. Crocitti, L. H. de Carvalho, S. C. Carroccio, P. Cerruti, and G. Santagata, "Properties of Biodegradable Films Based on Poly(butylene Succinate) (PBS) and Poly(butylene Adipate-co-Terephthalate) (PBAT) Blends," *Polymers* 12, no. 10 (2020): 2317.

32. A. M. Salaberria, R. H. Diaz, M. A. Andrés, S. C. M. Fernandes, and J. Labidi, "The Antifungal Activity of Functionalized Chitin Nanocrystals in Poly (Lactid Acid) Films," *Materials* 10 (2017): 546.

33. H. Al-Oufi, E. McLean, A. S. Kumar, M. Claereboudt, and M. Al-Habsi, "The Effects of Solar Radiation Upon Breaking Strength and Elongation of Fishing Nets," *Fisheries Research* 66 (2004): 115–119.

34. E. Grimaldo, B. Herrmann, N. Jacques, J. Vollstad, and B. Su, "Effect of Mechanical Properties of Monofilament Twines on the Catch Efficiency of Biodegradable Gillnet," *PLoS One* 15, no. 9 (2020): e0234224, https://doi.org/10.1371/journal.pone.0234224.

35. H. Fu, D. Yin, T. Wang, W. Gong, and H. Zhou, "Open Pore Morphology Evolution in Poly(Butylene Succinate)/Chitin Nanocrystal Nanocomposite Foams," *Journal of Polymers and the Environment* 30 (2022): 401–414.

36. Y. Ichikawa, H. Kondo, Y. Igarashi, K. Noguchi, K. Okuyama, and J. Washiyama, "Crystal Structures of a and b forms of poly(tetramethylene succinate)," *Polymer* 42 (2000): 4719–4727.

37. J. Xu and B. Guo, "Poly(Butylene Succinate) and its Copolymers: Research, Development and Industrialization," *Biotechnology Journal* 5 (2010): 1149–1163.

38. X. Wang, J. Zhou, and L. Li, "Multiple Melting Behavior of Poly(Butylene Succinate)," *European Polymer Journal* 43 (2007): 3163–3170.

39. U. S. Ishiaku, O. A. Khondker, S. Baba, A. Nakai, and H. Hamada, "Processing and Characterization of Short-Fiber Reinforced Jute/Poly Butylene Succinate Biodegradable Composites: The Effect of Weld-Line," *Journal of Polymers and the Environment* 13 (2005): 151–157.

40. G. Liu, L. Zheng, X. Zhang, C. Li, S. Jiang, and D. Wang, "Reversible Lamellar Thickening Induced by Crystal Transition in Poly(Butylene Succinate)," *Macromolecules* 45 (2012): 5487–5493.

41. Y. Ichikawa and T. Mizukoshi, "Synthetic Biodegradable Polymers," in *Advances in Polymer Science*, eds. B. Rieger, A. Künkel, G. W. Coates, R. Reichardt, and T. A. Dinjus (Springer, 2012), 285–313.

42. C. Wan, E. L. Heeley, Y. Zhou, et al., "Stress-Oscillation Behaviour of Semi-Crystalline Polymers: The Case of Poly(Butylene Succinate)," *Soft Matter* 14 (2018): 9175–9184.

43. K. Seonghun, K. Pyungkwan, J. Seongjae, and L. Kyounghoon, "Assessment of the Physical Characteristics and Fishing Performance of Gillnets Using Biodegradable Resin (PBS/PBATand PBSAT) to Reduce Ghost Fishing," *Aquatic Conservation* 30 (2020): 1868.

44. A. J. Crosby and J. Y. Lee, "Polymer Nanocomposites: The "Nano" Effect on Mechanical Properties," *Polymer Reviews* 47 (2007): 217–229.

45. M. Barletta, C. Aversa, M. Ayyoob, et al., "Poly(Butylene Succinate) (PBS): Materials, Processing, and Industrial Applications," *Progress in Polymer Science* 132 (2022): 101579.

46. F. Wu, M. Misra, and A. K. Mohanty, "Novel Tunable Super-Tough Materials From Biodegradable Polymer Blends: Nano-Structuring Through Reactive Extrusion," *RSC Advances* 9 (2019): 2836–2847.

47. O. Platnieks, A. Sereda, S. Gaidukovs, et al., "Adding Value to Poly (Butylene Succinate) and Nanofibrillated Cellulose-Based Sustainable Nanocomposites by Applying Masterbatch Process," *Industrial Crops and Products* 169 (2021): 113669.

48. S. E. Atalay, B. Bezci, B. Özdemir, et al., "Thermal and Environmentally Induced Degradation Behaviors of Amorphous and Semicrystalline PLAs Through Rheological Analysis," *Journal of Polymers and the Environment* 29 (2021): 3412–3426.

49. M. Hakkarainen, "Aliphatic Polyesters: Abiotic and Biotic Degradation and Degradation Products," in *Degradable Aliphatic Polyesters. Advances in Polymer Science* (Springer, 2002).

50. R. Muthuraj, M. Misra, and A. K. Mohanty, "Hydrolytic Degradation of Biodegradable Polyesters Under Simulated Environmental Conditions," *Journal of Applied Polymer Science* 132 (2015): 1.

51. V. A. Alvarez, A. N. Fraga, and A. Vázquez, "Effects of the Moisture and Fiber Content on the Mechanical Properties of Biodegradable Polymer–Sisal Fiber Biocomposites," *Journal of Applied Polymer Science* 91 (2004): 4007–4016.

52. Q. Wang, T. Chen, X. Wang, et al., "Recent Progress on Moisture Absorption Aging of Plant Fiber Reinforced Polymer Composites," *Polymers (Basel)* 15, no. 20 (2023): 4121, https://doi.org/10.3390/polym15204121.

53. J. P. Eubeler, M. Bernhard, and T. P. Knepper, "Environmental Biodegradation of Synthetic Polymers II. Biodegradation of Different Polymer Groups," *TRAC Trends in Analytical Chemistry* 29 (2010): 84–100.

54. F. V. Ferreira, L. S. Cividanes, R. F. Gouveia, and L. M. F. Lona, "An Overview on Properties and Applications of Poly(butylene Adipate-Co-Terephthalate)–PBAT Based Composites," *Polymer Engineering and Science* 59 (2019): E7.

55. H. Tsuji, *Bio-Based Plastics: Materials and Applications*, ed. S. Kabasci (John Wiley & Sons, Ltd, 2014), 171.